INSTITUTE OF PHYSICS PUBLISHING REPORTS ON PROGRESS IN PHYSICS

Rep. Prog. Phys. **67** (2004) 813–855 PII: S0034-4885(04)36784-9

The physics of attosecond light pulses

Pierre Agostini[1,3] **and Louis F DiMauro**[2]

[1] Commissariat à l'Energie Atomique, Direction des Sciences de la Matière, Centre d'Etudes de Saclay, 91191 Gif Sur Yvette, France
[2] Brookhaven National Laboratory, Chemistry Department, Upton, NY 11973, USA

E-mail: pagostini@cea.fr

Received 10 February 2004
Published 14 May 2004
Online at stacks.iop.org/RoPP/67/813
DOI: 10.1088/0034-4885/67/6/R01

Abstract

The word 'attosecond' (1 as $= 10^{-18}$ s) officially entered the vocabulary of physics when sub-femtosecond pulses of UV/XUV light produced either by nonlinear frequency conversion of a ultra-short infrared pump pulse or Fourier synthesis of broad bandwidth radiation were established. The physics of these pulses is based on nonlinear, nonperturbative laser–atom interaction: stimulated Raman scattering or high harmonic generation (HHG) is used to generate the necessary bandwidth, which naturally encompasses the visible and UV/XUV spectral range. However, the crucial element for attosecond pulse generation is the control of the spectral phase. New methods of temporal characterization at frequencies lying in the UV/XUV had to be elaborated. These methods rely on the energy/momentum analysis of photoelectrons produced by XUV attosecond flashes in the presence of an intense infrared field whose optical cycle itself becomes the basic clock. Single 650 as pulses have been produced and applied to trace the dynamics of electrons inside atoms following the creation of an inner-shell hole. Periodic combs of 250 as pulses have been synthesized by superposing just four harmonics and applying to the attosecond timing of the electron motion in HHG. Although it is easy to increase the bandwidth by coupling more harmonics, a fundamental limit to the duration of the light bursts produced has been discovered. It is imposed by the lack of synchronization of the different harmonic orders. The current limit is estimated to be 130 as. The latest advances include a direct autocorrelation of an attosecond pulse train and the production of a single 250 as soft x-ray pulse. This paper offers a snapshot of the state-of-the-art in the production and characterization of attosecond light pulses, with a glimpse at the first steps in attophysics.

(Some figures in this article are in colour only in the electronic version)

[3] Author to whom any correspondence should be addressed.

Contents

1. Introduction

1.1. The femtosecond barrier

The measurement of short time intervals and the perception of the dynamics of nature are largely dependent on light pulses. The need for finer time resolution and the quest for higher peak power explain the continuous trend towards shorter laser pulses almost since the inception of the laser. The historical progress of ultra-short technology is summarized in figure 1. The first pulsed lasers had durations of several hundreds of microseconds. Within a year or so, the invention of the Q-switch by Hellwarth (1961) reduced the pulse length to 10 ns, a four-order-of-magnitude decrease. Mode-locking (DeMaria *et al* 1966) accompanied by broad-gain dye laser media (Shank and Ippen 1974) further reduced the duration to less than 1 ps, another four orders of narrowing. The next three-order reduction took another 10–15 years to achieve. The main development was the ring cavity with intra-cavity prism compensation of the group velocity dispersion with which 6 fs pulses were produced (Fork *et al* 1987). From that date it could be said that the progress has been marginal. Although the replacement of dyes by Ti–sapphire, a solid-state gain medium, brought considerable changes in the size, performance, reproducibility and ease of operation of ultra-short laser systems, the wavelength was at the same time shifted to the near infrared (800 nm), where 5 fs long pulses are just a few cycles long[4]. By the end of the nineties, the innovations introduced by Kerr-lens mode-locking, self-phase modulation spectral broadening, the availability of chirped, ultra-broad band mirrors and pulse compression all led to pulse lengths of about two full cycles (Steinmeyer *et al* 1999). Clearly, given that a pulse of light should be at least one cycle long and that the Ti–sapphire optical period is 2.7 fs, the necessary prerequisite for attosecond light pulses is higher carrier frequencies.

1.2. Beyond the barrier: attosecond x-ray pulses

During the last decade, a scheme was slowly emerging that had the potential to break the femtosecond barrier: Fourier synthesis (FS) could possibly generate a pulse of a few attoseconds ($1\,\text{as} = 10^{-18}\,\text{s}$) and was proposed by Hänsch (1990), Farkas and Toth (1992) and Harris *et al* (1993). The basic idea is the production of a comb of equidistant frequencies in the spectral domain with controlled relative phases, thus mimicking the operation of a mode-locked laser. Hänsch (1990) proposed using sum and frequency mixing, while Farkas and Toth (1992) recognized that high harmonic generation (HHG) could easily produce a broad spectral domain in a series of lines separated by twice the fundamental frequency. Kaplan (1994) suggested another physical effect for obtaining a broad series of equidistant frequencies: cascaded stimulated Raman scattering (CSRS), to which is related the concept subsequently developed by Harris and Sokolov (1997, 1998)[5]. Both the harmonic and Raman routes have now proved to be successful, and in the case of HHG pulses as short as 130 as can be synthesized (Mairesse *et al* 2003). Clearly, the phase-locking of a periodic spectrum of equidistant frequencies can result only in a periodic intensity profile in the time domain, i.e. a comb (or 'train') of pulses. The 'extraction' of a single pulse from such a train is in principle possible, although its period is only about 1 fs, i.e. too fast for the usual electronic devices.

[4] Note that pulse durations are usually given as the full-width at half-maximum (FWHM) of the intensity profile. The field envelope is $\sqrt{2}$ longer for Gaussian envelopes. Thus a '5 fs' Gaussian pulse contains approximately two cycles at FWHM and six cycles at $1/e^2$.

[5] A somewhat similar method based on the modulation of the *linear* index of refraction in a Raman active medium has been shown recently to be effective in reducing femtosecond pulses (Wittmann *et al* 2000, Zhavoronkov and Korn 2002). It will not be discussed in this paper, which is focused on sub-femtosecond pulse generation.

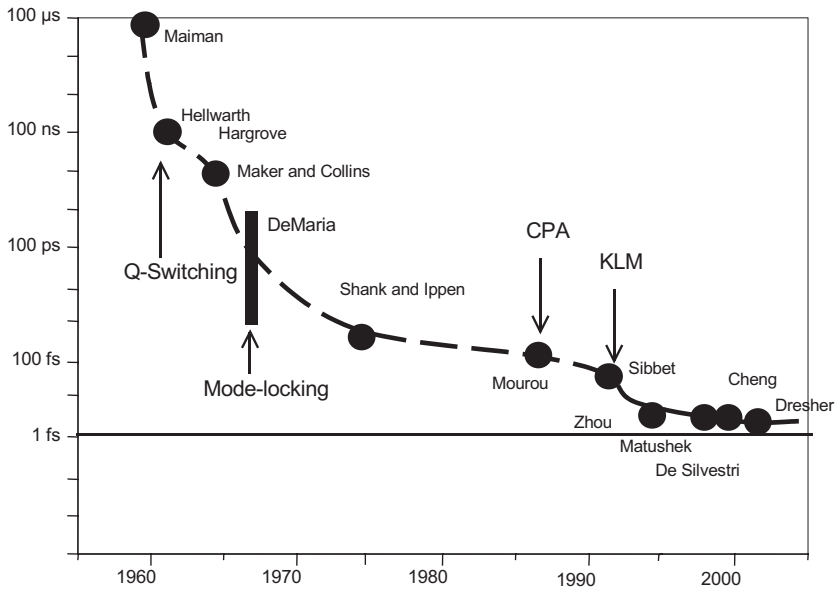

Figure 1. Timeline of the laser pulse length evolution from the free-running laser of Maiman to the recent refinements. A few names and techniques mark the essential steps in this evolution. The existence of a femtosecond barrier is clearly visible on the graph.

Ivanov *et al* (1995) and Platonenko and Strelkov (1999) proposed achieving sub-femtosecond harmonic pulses from a 'long' pump pulse by taking advantage of the high sensitivity of HHG to the pump light polarization. Tcherbakov *et al* (2003), Kovacev *et al* (2003) have put these ideas to work. More tempting is the production of a single sub-femtosecond pulse by harmonic generation with a few-cycle pump pulse: due to the high nonlinearity of the HHG process, a considerable temporal reduction of the harmonic pulse with respect to the pump is expected (and actually observed). Single pulses approaching 1 fs (Drescher *et al* 2001), a few hundreds of attoseconds (Hentschel *et al* 2001) and recently 250 as (Kienberger *et al* 2004) were reported. These numbers give an idea of how fast the field is progressing. The physics of both routes to attosecond pulse generation is outlined in section 2.

1.3. New metrology and new applications

Sub-femtosecond pulses not only require new methods of generation but also new methods of characterization. It is quite a challenge to measure attosecond pulses, which besides their extremely short duration have spectral components in the XUV range with a rather low intensity. Consequently, major obstacles prevent the application of standard short pulse metrology (autocorrelation, FROG, etc) utilizing nonlinear crystals since, unfortunately, absorption occurs in the XUV and the nonlinearity requires a sufficiently high intensity. Alternately, some novel methods rely on the photoionization of some target atom by the ultra-short XUV flash in the presence of an intense infrared electromagnetic *field* that is used as the basic clock (Kienberger *et al* 2002, 2004). Another method, known as RABITT, is particularly well adapted to the case of the discrete spectrum of a periodic train of attosecond pulses. Utilizing two-photon, multicolour ionization, the amplitudes and phases of the spectral components can be determined, thus allowing a reconstruction of an average temporal profile (Paul *et al* 2001,

Mairesse *et al* 2003). In a very recent experiment, direct second order autocorrelation of an attosecond pulse train was achieved (Tzallas *et al* 2003). In section 3 the characterization methods are reviewed along with the current status of the attosecond pulse generation.

One of the primary goals of attosecond science is to provide more insights into the dynamics of atomic electrons. Although in its infancy, the field of attophysics is beginning to emerge, and a few seminal experiments have paved the way. One general interest is the direct probing in time of hyperfast electronic rearrangements following the creation of an inner-shell hole. A demonstration of this spectroscopy has been reported recently (Drescher *et al* 2002) using a pump–probe approach. Another study using sub-femtosecond burst of XUV light (Kienberger *et al* 2002) probed the motion of an electron wave packet under the influence of an infrared laser's electric field. Furthermore, the precise timing of the electron wave packet emitting the high harmonics can be measured by observing the two-photon ionization electron energy spectrum (Aseyev *et al* 2003, Dinu *et al* 2003). These pioneering experiments are reviewed in section 4.

What are the limits and future of attosecond pulses? It has been established recently (Mairesse *et al* 2003) that a fundamental lack of synchronization at the level of the single atom response imposes a lower limit to the pulse duration generated by superposition of high harmonics. Section 5 addresses this issue and other questions regarding the limits of attosecond pulse generation.

Finally, section 6 examines other proposals for generating attosecond pulses and the prospects of producing even shorter pulses approaching the nuclear timescale.

2. Theory of attosecond pulses

2.1. Background

The idea (Hänsch 1990) of using FS to engineer short pulses is derived from the principle of the mode-locked laser: if N spectral modes within the gain bandwidth are phase-locked, then the temporal profile is a sequence of pulses separated by the cavity round-trip time, each with a duration $\propto 1/N$. In the laser, the frequency range is limited to the gain bandwidth ($\sim$100 THz). To support a 100 as pulse, a bandwidth of 5×10^3 THz or about 40 eV is necessary. Various methods for generating a wide sequence of equidistant frequencies utilizing nonlinear processes have been discussed: Hänsch (1990) has proposed generating six frequencies by sum and difference frequency generation. A much broader span of frequencies is available in HHG, a process discovered a decade earlier (McPherson *et al* 1987, Ferray *et al* 1988). In HHG, an intense laser pulse of carrier frequency ω_L focused into a jet of rare gas atoms generates a comb of odd-order harmonics with frequencies $q\omega_L$ ($q = 3, 5, \ldots$) and nearly equal *amplitudes* over a large spectral range dubbed the 'plateau', followed by a rapid decrease in the 'cutoff' region (Krause *et al* 1992, Salières *et al* 1999) (see figure 2). Assuming equal phases among the harmonics, Farkas and Toth (1992) first predicted that the intensity temporal profile obtained by coherently superposing N harmonic orders would produce ($\propto 1/N$), narrow bursts twice per optical period of the fundamental, $2\pi/\omega_L$, with peak intensities $\propto N^2$. A similar idea has been proposed by Harris *et al* (1993).

Another route to FS of ultra-short pulses has been proposed by Kaplan (1994). Arguing that HHG process is inherently inefficient, producing pulses with energies many orders of magnitude lower than that of the driving field, he proposed synthesizing sub-femtosecond pulses by superposing the frequencies generated by CSRS. In theory, the CSRS process would be more efficient than HHG, while producing equally spaced frequency components with locked phases. In the stimulated Raman scattering (SRS) scheme a large fraction of the input

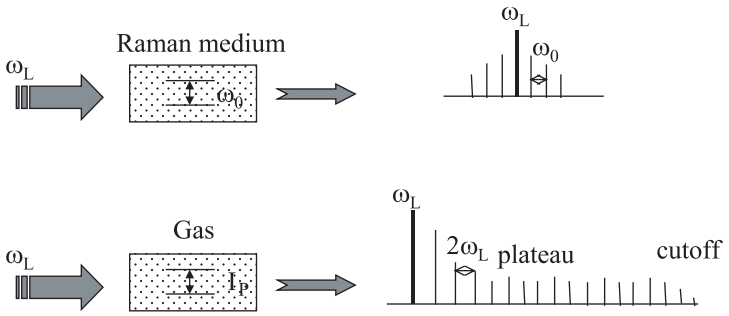

Figure 2. Raman scattering versus HHG. In Raman scattering, the medium is characterized by a Raman frequency which is also the period of the Stokes and anti-Stokes spacings on both sides of the input frequency. In the HHG this spacing is twice the input photon energy. I_p is the ionization potential of the atom. The cutoff frequency is about $3U_p + I_p$ if U_p is the ponderomotive energy associated with the input pulse intensity I and photon energy ω: $U_p = I/4\omega^2$ in atomic units.

energy is converted into the sidebands, while in HHG the conversion efficiency is at most 10^{-5}. A variant of this idea was implemented by Harris and Sokolov (1997): using two lasers with frequencies separated by the Raman shift of the medium a broad frequency comb necessary for attosecond generation was produced.

The SRS and the HHG methods described in the next sections have in common that in both, the frequency comb (the 'sidebands') is engineered by the nonlinear interaction between an intense laser pulse and a vapour[6]. The comb period is ten times smaller for SRS (typically 100 THz) than for HHG (1000 THz), and both generate spectra extending into the UV/XUV, but HHG produces significantly higher carrier frequencies. The fact that many frequencies of the SRS comb lie in the visible spectrum makes the phase control of these spectral components much simpler to implement than for HHG. An alternate strategy for studying attosecond pulse generation using high harmonic light has been demonstrated at Brookhaven (Sheehy *et al* 1999, Clatterbuck *et al* 2003, 2004). In order to circumvent the difficulties associated with the metrology of harmonics produced in the XUV spectral region, a mid-infrared fundamental field is used to produce a high harmonic comb in the visible and near-ultraviolet. Consequently, this approach has practical advantages similar to those of the SRS method, while mimicking the physics of the short wavelength HHG process.

2.2. Generation of Raman sidebands

2.2.1. CSRS soliton. It has long been known that SRS can create equidistant frequencies on the Stokes and anti-Stokes sides of the pump frequency. The question of the phase-locking has however been an open question. Kaplan (1994) established theoretically that a Raman medium, characterized by a Raman shift ω_0, can generate mode-locked equidistant frequencies that result in a train of pulses separated by $2\pi/\omega_0$ and resemble a self-induced transparency soliton (McCall and Hahn 1967), i.e. propagates without deformation over large distances. The medium, upon exposure to intense light at frequency ω_1, generates Stokes and anti-Stokes frequencies $\omega_1 \pm n\omega_0$ (figure 3). The Raman transition is described by the nondiagonal elements, $\rho_{12} = \rho_{21}^*$, of the density matrix. The total Raman field is the sum over M_A, anti-Stokes, and M_S, Stokes, components plus the input frequency component propagating collinearly in the medium. A set of Maxwell equations for the amplitude of the jth field

[6] See footnote 5.

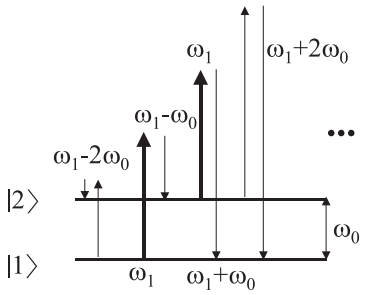

Figure 3. Energy level scheme for the formation of SRS sidebands in a Raman medium with the Raman shifted frequencies $\omega_1 \pm n\omega_0$ from which the sub-femtosecond solitons are synthesized.

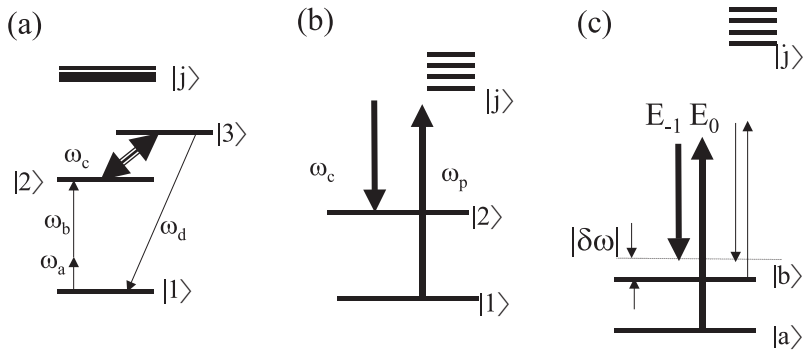

Figure 4. Energy level schemes illustrating (*a*) EIT, (*b*) a related scheme in which ω_p is the pump beam and ω_0 the coupling laser frequencies, (*c*) the stimulated Raman scheme in which two input frequencies are noted E_0 and E_{-1}. The Raman shift is ω_0 and $\delta\omega = (E_0 - E_{-1} - \omega_0)$ is the small detuning (see section 2.2.2).

component coupled to the $(j \pm 1)$ ones is obtained, assuming that the nondiagonal density matrix elements have the form $\rho_{12} = (\mathrm{i}/2)\sigma(t, z)\exp\mathrm{i}(k_0 z - \omega_0 t)$. It can be shown that the evolution of the density matrix is governed by the generalized Bloch equations, which depend on a generalized Rabi frequency:

$$\tilde{\Omega}_{\mathrm{R}} = 2\sum_{j=-M_{\mathrm{S}}}^{M_{\mathrm{A}}-1} \alpha_{j,j+1} E_j E_{j+1}^{*} \tag{1}$$

where $\alpha_{j,j+1}$ involves the Raman nonlinear coefficients and the phase mismatching of the j and $j+1$ components. From there it can be established that a stationary wave is a solution of the set of equations and that all the components are *phase-locked* to each other. A numerical investigation of a model medium shows the emission of a sequence of sub-femtosecond (approaching 200 as) pulse trains. In spite of its simplicity, this scheme has not been put in practice, to our knowledge. The method discussed in the next section on the other hand, closely related to the CSRS, has been implemented successfully.

2.2.2. Molecular index modulation through SRS. The inception of this scheme can be traced to two seminal ideas: electromagnetically induced transparency (EIT) (Harris *et al* 1990) and the CSRS, discussed in the previous section. The basic scheme of the EIT is shown in figure 4(*a*). Harris *et al* (1990) have shown that by applying a strong coupling between a

metastable state $|2\rangle$ and the upper state $|3\rangle$ of an allowed transition to the ground state, one may obtain a resonantly enhanced third-order susceptibility, while at the same time inducing transparency of the medium at the transition frequency, ω_d. The transparency occurs because of a destructive interference of the split components (Autler-Townes) of the transition and a constructive interference for the nonlinear susceptibility. Harris (1994) has also shown that an analogous scheme (shown in figure 4(*b*)), allows control of the refractive index of a weak probe beam by introducing a strong coupling laser. The method of generating a wide spectrum and at the same time improving the propagation through a gaseous medium is derived from that idea (Harris and Sokolov 1997). It is based on using a small two-photon detuning from a Raman resonance to generate a broad spectrum of sidebands (as shown in figure 4(*c*)). Although this scheme bears a resemblance to the CSRS of section 2.2.1, it differs from it in the fact that two input frequencies are needed. These two frequencies are slightly detuned from the Raman transition, and the system is driven between the molecular vibrational states by the strong two-photon coupling caused by the two lasers at frequencies E_0 and E_1 with a Rabi rate proportional to the product of the two input fields. The coherent molecular oscillation modulates the medium refractive index, which in turn induces laser frequency modulation and hence the buildup of sidebands whose total bandwidth extends over the infrared, visible and UV spectral regions. The set of Raman sidebands self-consistently establish the molecular coherence and propagate without change of amplitude or phase. In other words, periodic trains of femtosecond timescale optical pulses may propagate in a dispersive medium without changing shape (Yavuz *et al* 2000). Analogous to the three-level EIT system, sufficient pulse energy is required to establish the molecular coherence, but a large fraction of this energy is converted into the sidebands. Several experiments described in section 3 confirm these theoretical predictions and demonstrate the generation of pulses approaching 1 fs duration.

2.3. High harmonic generation

HHG seems, at first glance, to offer an easier method for producing attosecond pulses by FS. An intense infrared laser pulse focused in an atomic or molecular vapour induces coherent emission of odd-order harmonics with very high orders: a 800 nm Ti–sapphire laser can produce wavelengths down to a few nanometres (Chang *et al* 1997, Schnürer *et al* 1998). Furthermore, only a small fraction of the generate spectral range is sufficient for forming sub-femtosecond pulse trains, provided the phases are locked. Moreover, the HHG produced by sub-10 fs fundamental fields is a likely route to a *single* attosecond XUV pulse.

2.3.1. The three-step recollision model of HHG. Starting with the first observation of HHG in the laboratory, it was immediately clear that the process was not perturbative. The most conspicuous symptom in the HHG spectrum shown in figure 5 is the long 'plateau' of constant amplitude over a large spectral range, instead of the normal rapid drop with order expected from perturbation theory. The physical origin of this behaviour is contrary to the perturbative situation, where the electron undergoes a small, slightly anharmonic motion. In a strong field, $E_0 \sin \omega t$, the electron is freed in a fraction of the optical cycle, $2\pi/\omega$, and undergoes a large amplitude (E_0/ω^2) oscillation, acquiring a large kinetic energy that may be released as a high energy harmonic photon during a recollision with the core. The various harmonic frequencies correspond to different field-driven electron trajectories resulting in different kinetic energies at the recollision time. This intuitive classical model is known as the 'rescattering' model (Schafer *et al* 1993) or the 'three-step recollision' model of harmonic generation (Corkum 1993). An early quantum version, the 'atomic antenna' model of Kuciev (1987), was expanded by Lewenstein *et al* (1994) into a more convenient approach. Although it has been abundantly

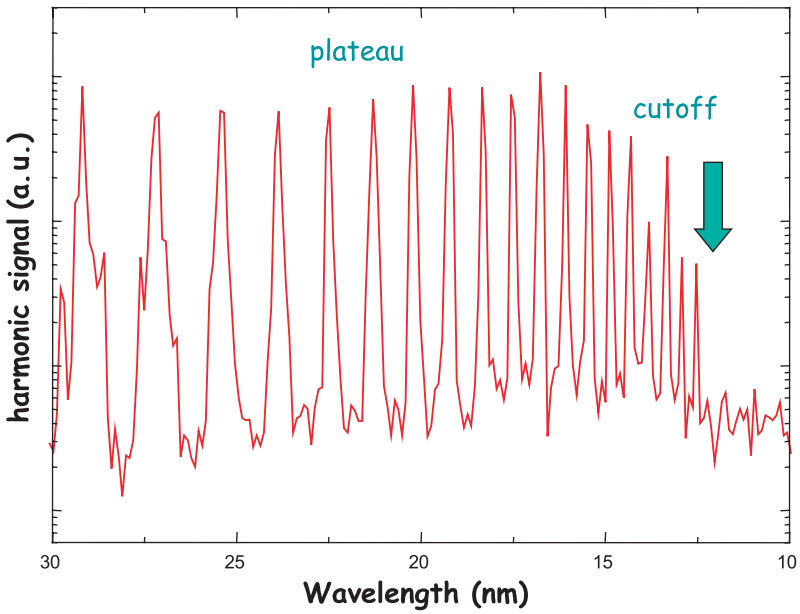

Figure 5. A partial high harmonic spectrum from neon irradiated by 50 fs, 800 nm pulses versus wavelength. In energy the corresponding peaks are equidistant and separated by 3.1 eV twice the Ti–sapphire photon energy. The graph clearly shows the plateau and cutoff characteristics of this type of emission. The cutoff occurs in this case for orders higher than 61. The lowest order on the left of the picture is the 27th.

discussed in the literature, it will be sketched here briefly since it provides a convenient basis for understanding the intensity-dependent phase that is crucial for the formation of attosecond pulses.

Given a single atom in a classical electromagnetic field, the Schrödinger equation can be solved using the following approximations: (a) all atomic states except the ground state and the continuum are ignored, (b) the depletion of the ground state is neglected and (c) the electron in the continuum state, labelled by the momentum of the outgoing electron, $|\boldsymbol{v}\rangle$, is treated as a free particle moving in an electric field, i.e. the atomic potential is ignored. Using these three assumptions, the wave function is expanded as

$$|\Psi(t)\rangle = \mathrm{e}^{\mathrm{i}I_\mathrm{p}t} \mid a(t)|0\rangle + \int \mathrm{d}^3\boldsymbol{v}\, b(\boldsymbol{v},t)|\boldsymbol{v}\rangle \tag{2}$$

where $a(t) \approx 1$ and $b(\boldsymbol{v},t)$ are the ground and continuum state amplitudes, respectively, and I_p is the atomic ionization potential. The Schrödinger equation in the length gauge can then be solved exactly and the time-dependent dipole moment can be evaluated as

$$x(t) = \langle\Psi(t)|x|\Psi(t)\rangle = \int \mathrm{d}^3\boldsymbol{v}\, d_x^*(\boldsymbol{v})b(\boldsymbol{v},t) + \mathrm{c.c.} \tag{3}$$

where $d(\boldsymbol{v}) = \langle\boldsymbol{v}|x|0\rangle$ denotes the bound-free unique matrix element of the problem. The harmonic spectrum in this framework is the Fourier transform of $x(t)$. Owing to the properties of the dipole matrix elements due to the central symmetry of the atomic potential, only odd harmonics survive. Introducing the canonical momentum,

$$\boldsymbol{p} = \boldsymbol{v} + \boldsymbol{A} \tag{4}$$

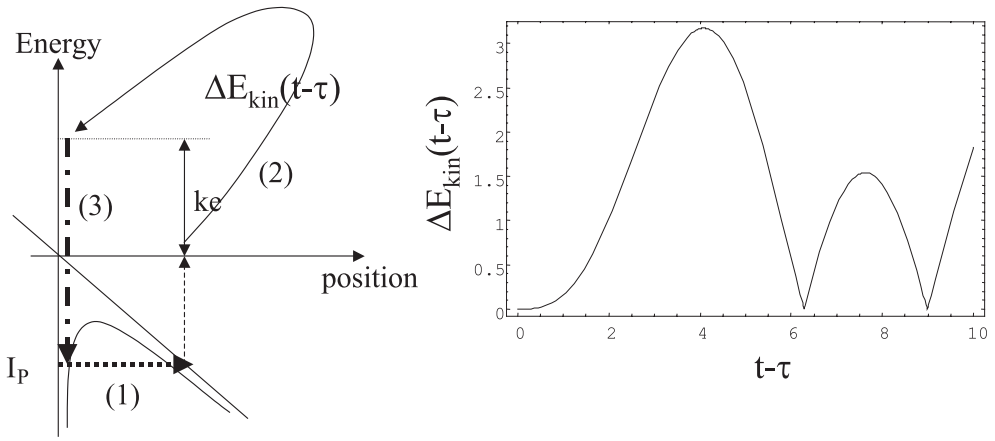

Figure 6. The left part of the figure illustrates the three-step recollision model: (1) tunnelling; (2) classical trajectory under the influence of the electromagnetic field practically alone. During this part the electron acquires a kinetic energy (and its wavefunction a phase); (3) recombination in which the kinetic energy acquired in (2) plus the ionization energy I_p overcome in (1) are converted into a high energy photon. The right part of the figure shows the classical kinetic energy (in units of the ponderomotive energy U_p versus the return time, showing in particular the maximum at 3.2, which accounts for the harmonic cutoff $3.2U_\mathrm{p} + I_\mathrm{p}$. In the fully quantum version, the electron wavefunction keeps a trace of the classical trajectory (2) as a phase given by the quasi-classical action (see section 2.3.1).

the dipole can be written as

$$x(t) = \mathrm{i}\int_0^t \mathrm{d}\tau \int \mathrm{d}^3\boldsymbol{p}\, E\cos(\tau) d_x(\boldsymbol{p} - \boldsymbol{A}(\tau)) \exp[-\mathrm{i}\boldsymbol{S}(\boldsymbol{p}, t, \tau)] \times d_x^*(\boldsymbol{p} - \boldsymbol{A}(t)) + \mathrm{c.c.} \qquad (5)$$

with

$$S(\boldsymbol{p}, t, \tau) = \int_\tau^t \mathrm{d}t' \left(\frac{[\boldsymbol{p} - \boldsymbol{A}(t')]^2}{2} + I_\mathrm{p} \right). \qquad (6)$$

Equation (5) can be interpreted as a sum of probability amplitudes of the following processes: (1) the first term in the integral $E\cos(\tau)d_x(\boldsymbol{p} - \boldsymbol{A}(\tau))$ is the electron's transition amplitude from the ground state at time τ to the continuum with a canonical momentum $\boldsymbol{p}$. (2) The wave function then propagates from τ to t and acquires a phase factor $\exp[-\mathrm{i}S(\boldsymbol{p}, t, \tau)]$, where $S(\boldsymbol{p}, t, \tau)$ is the quasi-classical action given by equation (6). (3) Finally, the electron recombines with its parent ion at time t with the probability amplitude $d_x^*(\boldsymbol{p} - \boldsymbol{A}(t))$. One can identify easily in this formalism the three steps of the semi-classical model illustrated in figure 6. Without going into any more details, it is clear that the major contributions to the integral in equation (5) come from the stationary points of the classical action, i.e. the classical trajectories,

$$\nabla_{\boldsymbol{p}} S(\boldsymbol{p}, t, \tau) = 0. \qquad (7)$$

The dominant contribution to the harmonic emission originates from the electrons that tunnelled into the continuum and returned to the vicinity of the nucleus due to the laser field acceleration. It can be shown that for each harmonic, the main contributions come from two trajectories with degenerate kinetic energy (see figure 6) at the core position, the so-called 'long' and 'short' trajectories illustrated in figure 7. The dipole from equation (5) is a complex number and therefore has a phase that is determined by the action acquired along the classical trajectories, i.e. $\sim U_\mathrm{p}(t - \tau)$, where U_p is the ponderomotive energy, given in atomic units

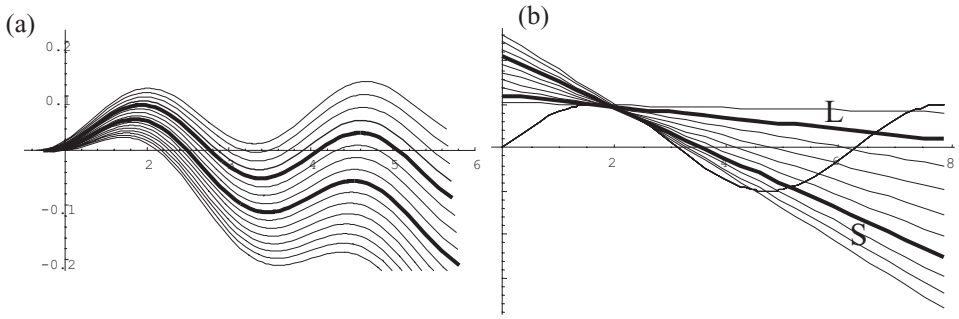

Figure 7. Free electron trajectories $x(t)$ in a monochromatic electromagnetic field: (*a*) in the laboratory frame; (*b*) in the frame oscillating at the field frequency (Kramers–Henneberger frame) in which the electron moves in straight lines. The nucleus motion is then a sine curve. An electron leaves the nucleus at the emission time with a velocity given by the tangent to the sine function. It may recollide with the nucleus if the tangent at the initial point encounters the sine function at some later time. Each kinetic energy at the impact with the nucleus can be reached along two trajectories corresponding to slightly different emission times: the so-called short (S label)and long (L label) trajectories, the name referring to the time difference between the emission and recollision times.

as $E^2/4\omega^2$. Calculations (Lewenstein *et al* 1995) show that the phase is $\approx -3.02U_p$ for the plateau harmonics.

2.3.2. Harmonic phases and attosecond pulses. Obviously, the phase parameter is of utmost importance for the production of attosecond pulses. Since, according to the theory, the phase $\sim U_p(t - \tau)$ is a linear function of intensity, which for a focused laser pulse is a function of time and space, the prospects of maintaining a constant phase difference between the harmonics were *a priori* rather poor. The first realistic calculation of the temporal profile resulting from the superposition of plateau harmonics (Antoine *et al* 1996) showed that nature was fortunately cooperating. The calculation revealed that the temporal profile obtained by the superposition of 10 plateau harmonics resulted in the emergence of four harmonic bursts within one optical cycle. This emission correlates in pairs to the 'short' and 'long' trajectories discussed earlier. The surprising result is that when the propagation inside the medium is taken into account, one or the other contributions can be eliminated, depending on experimentally controllable parameters. For example, the position of the atomic medium is assumed to be small in comparison with the beam's Rayleigh range, with respect to the focal plane. The resulting profile is predicted to consist of only *two* 120 as bursts per fundamental optical cycle (shown in figure 8). These lucky effects of phase-matching (L'Huillier *et al* 1991) can be understood as the interplay between the geometrical phase shift of the fundamental across the focus (the Gouy phase) and the variation of the dipole phase that follows the intensity distribution (Salières *et al* 1995). The roadmap for attosecond pulse generation was indeed opened by this seminal article, and, as will be shown later, the prediction was confirmed qualitatively by experiment. The influence of the spatio-temporal intensity distribution for a realistic experiment was analysed in more detail by Gaarde and Schafer (2002). The conclusion was that there exist conditions under which the production of a phase-locked train is robust. However, Gaarde and Schafer warned that both spatial and temporal phase variations of the harmonics must be taken into account.

Besides, the instantaneous frequency of the harmonics is actually determined by the phase time-derivative. For a Gaussian pulse, the phase is also Gaussian ($\propto$ intensity) and therefore the model predicts a linear chirp, which has consequences on the temporal envelope of the harmonic

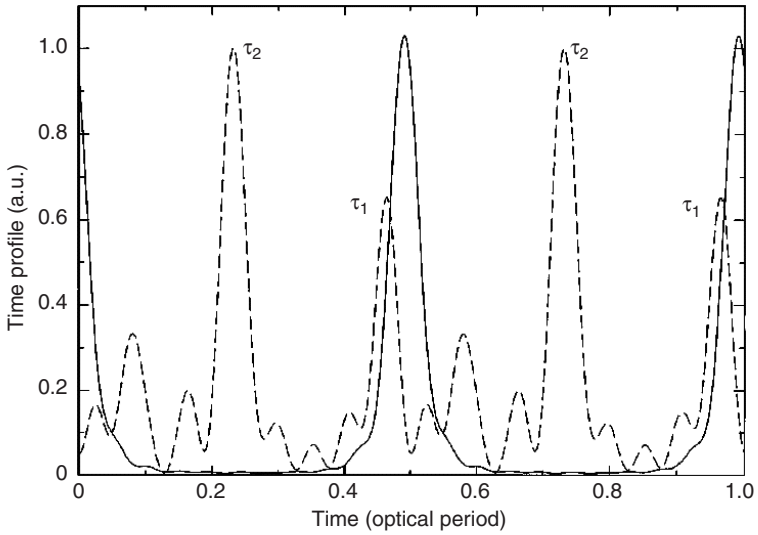

Figure 8. Theoretical harmonic intensity temporal profile obtained by summing 10 harmonics (41–61). The dashed line is the single atom response, the solid line the intensity resulting from a macroscopic sample. τ_1 and τ_2 refer to the short and long electron trajectories (see figure 7). The calculation clearly shows that one of the intensity peaks is eliminated by the propagation through the sample leaving only two bursts per optical period of the pump field. The experiment of Paul *et al* (2001) was in agreement with this prediction.

pulses (on the femtosecond scale) (Salières *et al* 1995, Bouhal *et al* 1998). From the attosecond pulses standpoint, if the chirp depends on the harmonic order, it would obviously affect the interference leading to the pulse train. If, on the contrary, the chirp is order-independent and small, it would lead to a mere translation in time.

Furthermore, the semi-classical model has a prediction that had been overlooked until the experiments of Mairesse *et al* (2003): the trajectories leading to different kinetic energies (harmonic orders) have different return times. This lack of sychronization of the different harmonic orders imposes a fundamental limitation on the attosecond pulses synthesized by HHG.

2.4. Generation of a single attosecond pulse

The generation of a train of attoseconds, which is the Fourier transform of the periodic spectrum of harmonics or Raman sidebands, does not require particularly short pump pulses. For many applications it may be desirable to reduce the train to a single pulse either by some kind of time-gating process (similar to the extraction of a single pulse from a mode-locked train by a Pockels cell) or by reducing the pump pulse itself.

2.4.1. Temporal confinement of harmonic emission: polarization gating. Harmonic generation is very sensitive to the ellipticity of the pump light and decreases rapidly as soon as the polarization departs from linear. From the classical standpoint of the recollision model, elliptically polarized light causes the electron wave packet to acquire a transverse velocity, thus never returning to the core. Therefore, if the polarization of the pump pulse is streaked rapidly from circular to linear and circular again, the effective pump time is reduced accordingly. This idea, initially proposed by Ivanov *et al* (1995) using two wavelengths

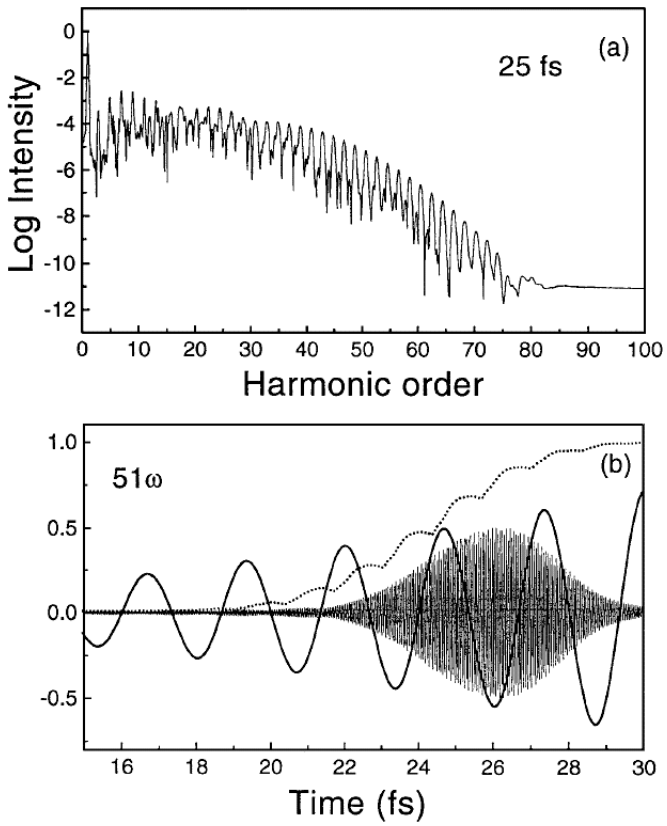

Figure 9. Calculated (*a*) high harmonic spectrum; (*b*) time profile of harmonic 51 in the case of a very short pump pulse. Note that the harmonic pulse (the rapidly oscillating curve) occurs during the rising edge of the pump pulse (slowly oscillating curve). Its prompt turn off in this case is due to the total depletion of the ground state indicated by the third curve in the plot.

and by Platonenko and Strelkov (1999) with a single wavelength is very attractive. It has been implemented and explored recently (Kovacev *et al* 2003, Tcherbakov *et al* 2003), and encouraging results have been obtained. Two quartz quarter-wave plates are sufficient for creating the polarization gate: the first one creates two replicas of the initial linearly polarized pump pulse with orthogonal polarizations and delayed by 31.3 fs. The second one generates a right and a left circularly polarized pulse separated by the same delay. During the time the two pulses overlap, the polarization is linear. With this device, Tcherbakov *et al* (2003) have reported for instance a temporal confinement of the harmonic emission on a 7 fs timescale with a pump pulse of 35 fs. Although it is problematic to obtain sufficient harmonic yield in such a time-dependent polarization pulse, this result seems reasonably promising.

2.4.2. Harmonic generation from a few-cycle pump pulse. The other natural route for attosecond generation using high harmonics is excitation with an *ultra-short* (i.e. a few-cycle) pump pulse. Due to the highly nonlinear dependence of HHG on the pump intensity, theory predicts the possibility of generating a *single* XUV burst (Christov *et al* 1997, Brabec and Krausz 2000). The reasons for a strong reduction of the harmonic pulse duration with respect to the fundamental pulse are multiple: they involve the nonlinear dependence of the dipole,

the phase mismatch due to the intensity-dependent phase in a space–time intensity distribution and the ionization depletion of the ground state (as shown in figure 9). As will be discussed below, experiments have confirmed that this is a very efficient route insofar as the required few-cycle pump pulse is available.

3. Attosecond pulses in the laboratory

The following section deals with the current status of attosecond pulse production. The technology needs are so novel and the progress so rapid that the crafting and the measurements had to be developed in unison. Consequently, the proof of existence was reported at the same time the corresponding new methods of characterization were validated. Currently, many groups are working intensively on this problem, and the following discussion represents only a transient state of things. As already mentioned, the techniques for generating attosecond light pulses can be divided into two groups: the FS of a pulse train, from Raman scattering or HHG or the direct production of a single attosecond pulse from a few-cycle pump pulse. The following subsections are organized in this manner.

3.1. Attosecond metrology: general considerations

The metrology of attosecond pulses is a difficult task: not only are the pulses too short for any electronic devices but their spectrum, in many cases, lies in the UV/XUV range, where the usual nonlinear material cannot be used. The lack of electronics with fast response has long been overcome by techniques like field/intensity autocorrelation or cross-correlation. The principle is to measure the convolution of the pulse to be characterized either with itself or with a known reference pulse. In order to estimate the pulse duration, these techniques require a beforehand knowledge that the pulse is 'short' and some hypothesis on the intensity profile's analytical shape. These techniques are 'incomplete' in the sense that they do not retrieve the field itself but only a function of this field. There is no inversion algorithm nor unicity for these methods. As rudimentary as they are, they cannot be applied directly in the XUV range. It is perhaps not inappropriate to recall that no linear method using an integrating detector can ever characterize a short pulse. An integrating detector is sensitive only to the spectral density of energy, any linear combination of the pulse with itself yields a signal $\propto \int |R_1(\omega)E(\omega) + R_2(\omega)E(\omega)|^2 \,\mathrm{d}\omega \propto |E(\omega)|^2$, which obviously contains no phase information. Thus a field autocorrelate is equivalent to measuring the power spectrum of the pulse. Nonlinear conversion, like second harmonic generation, is used to obtain interferometric or intensity autocorrelation or cross-correlation measurements. If the pulse to be characterized has sufficient intensity, multiphoton ionization of a gas can be used to provide a correlation signal and will be discussed later. In the general case, however, characterization of weak UV/XUV pulses relies on two-colour atomic ionization as the only usable nonlinear process. Cross-correlation methods based on this approach had been used for some time to measure femtosecond XUV/x-ray pulses (Schins *et al* 1994, 1996, Glover *et al* 1996). The variations of this principle include practically all the methods used today.

3.2. FS of attosecond pulse trains from SRS: cross-correlation through multiphoton ionization

In the case of the coherent superposition of sidebands generated by stimulated Raman modulation of the molecular refractive index, the resulting intensity is sufficient to induce multiphoton processes that can in turn be used to characterize the pulse train. The

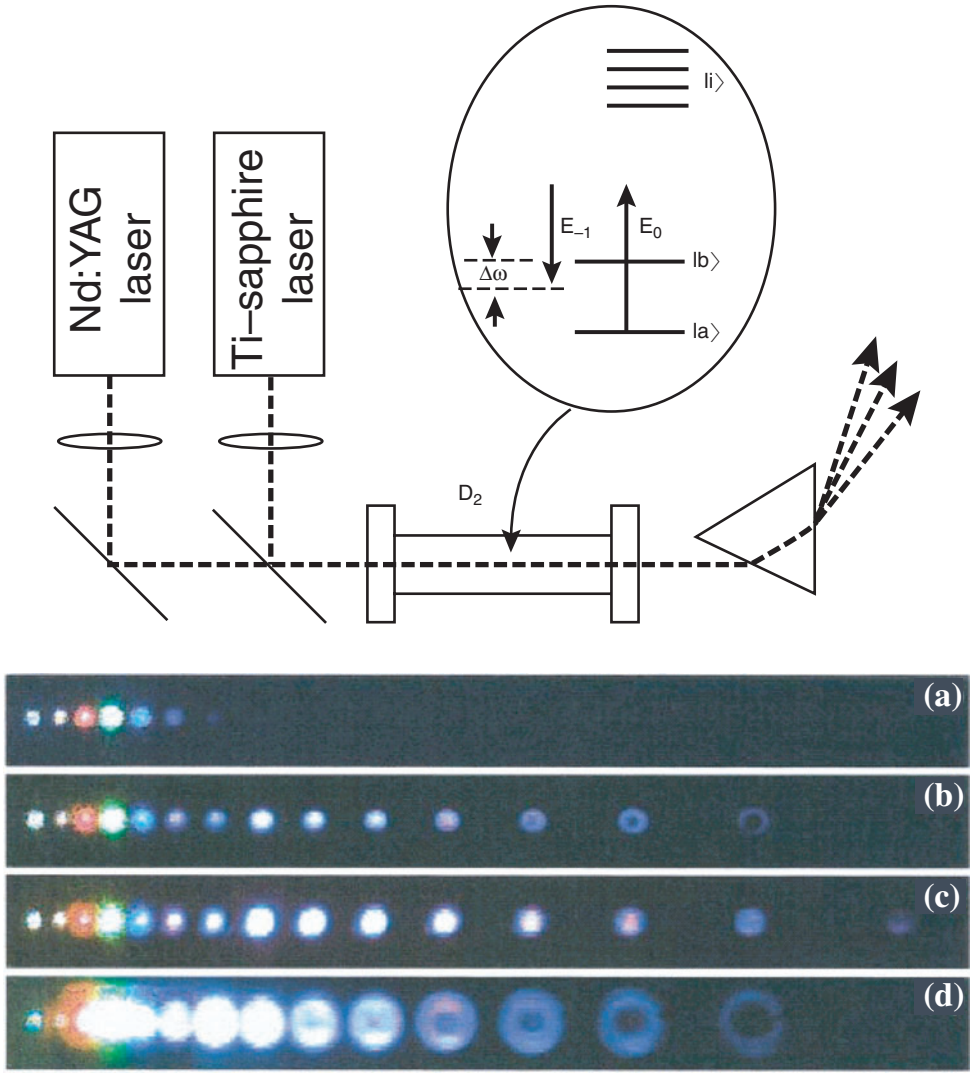

Figure 10. Raman spectrum generated by irradiating a deuterium cell by two lasers whose photon energies, 1.17 and 1.55 eV differ by a quantity (0.38 eV) close to the Raman shift corresponding to the fundamental vibration energy of D_2 (0.37 eV). The various sidebands are spectrally separated by a quartz prism since they lie in the visible/UV domain.

demonstration was made with sidebands generated in deuterium irradiated by a YAG laser ($\lambda = 1064.5$ nm) and a Ti–sapphire laser ($\lambda = 807.22$ nm) by Sokolov *et al* (2000, 2001a, b). The corresponding frequency difference, $\omega_a - \omega_b$, is close to the vibration frequency of deuterium ($2994\,\mathrm{cm}^{-1} \approx 90$ THz). As shown in figure 10, as many as 17 Stokes and anti-Stokes sidebands were observed, covering a range over $50\,000\,\mathrm{cm}^{-1}$ spaced by 90 THz and emitted collinearly with the incident laser beams. The control parameters of the emission are the detuning $\Delta\omega$ (positive or negative) and the deuterium pressure. The sidebands are theoretically expected to be mutually coherent and Sokolov *et al* (2001a, b) verified this by controlling the relative phases of three sidebands through an optical delay line and checking that the intensity of a fourth one was a sinusoidal function of this phase. The same authors

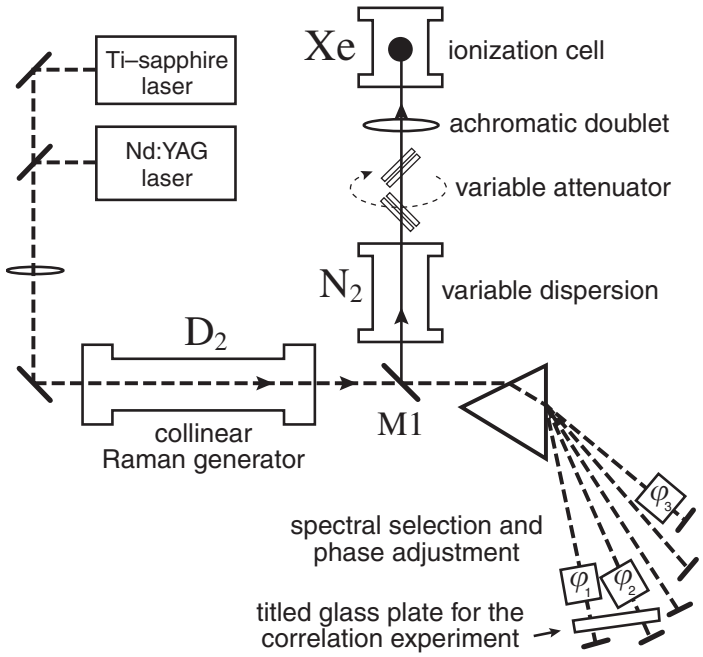

Figure 11. An experiment with the SRS source of figure 10. The various sidebands are phase controlled by adjusting the mirrors that reflect them back into the prism and from there into the experiment chamber. The phases are set for synthesizing the pulses shown in figure 12.

(Sokolov *et al* 2001a, b) also successfully synthesized waveforms containing optical bursts approaching one cycle by superposing five phase-controlled sidebands (1060, 807, 650, 544 and 468 nm). The waveform resulting from this superposition was extracted from the six-photon ionization of xenon (ionization potential = 12.13 eV) atoms, which is very sensitive to the pulse shape and can therefore be used to cross-correlate the synthesized pulse. The experiment measured the Xe^+ signal as a function of a delay introduced between two sidebands and the three others by a tilted glass plate (figure 11). The result demonstrated a good mutual coherence among the sidebands, which, when the phases were locked, resulted in a 2 fs (1 cycle) burst (figure 12).

The main advantage of Harris–Sokolov's method for producing sub-cycle pulses is that essentially all the pump power is converted into sidebands, while in HHG only a fraction of the order of 10^{-5} is transformed into high frequencies. Another clear advantage is that since many sidebands lie in the visible or near UV, the phase control through optical delay can be done in air and is very simple to implement. The drawback is that the burst's carrier wavelength lies in the visible and therefore might be less appealing for a number of applications requiring shorter duration pulses, which are more easily obtained with the HHG process.

It should be noted that the possibility of generating *single* sub-femtosecond pulses from high-order SRS exists, at least in theory (Kalosha and Herrmann 2000). The proposed scheme involves, besides the Raman medium and the two pump pulses discussed above, a third femtosecond probe pulse that experiences a large spectral broadening and a corresponding temporal shortening. However, the predicted pulse reduction by a factor of 5 for a typical input pulse of 20 fs places this scheme more as a competitor of the standard self-phase modulation/compression techniques in hollow core fibre optics than an actual attosecond source. This proposal has not been yet realized, to our knowledge.

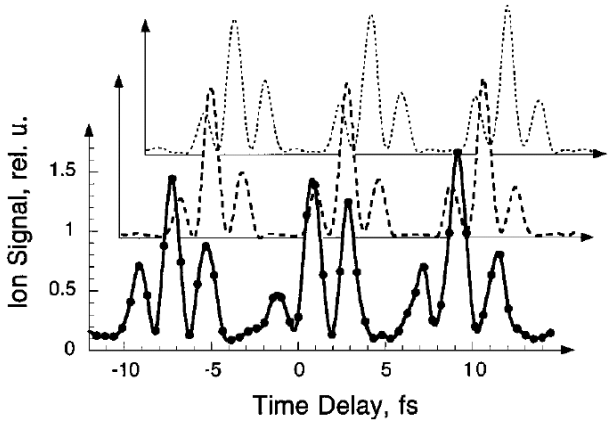

Figure 12. The temporal profile of the pulse train resulting from the superposition of the Raman sidebands (——) is determined by cross-correlation using multiphoton ionization as a nonlinear signal. The shortest pulse is about 1 fs, in good agreement with the calculation (· · · · · and - - - -).

3.3. FS of attosecond pulse trains from HHG

Although a decade of different theoretical approaches have hinted at the existence of attosecond pulses from HHG (see section 2), the experimental evidence has been found only recently.

3.3.1. Field autocorrelation. The first claim of attosecond pulses resulting from the superposition of high harmonics was made by Papadogiannis *et al* (1999). A 60 fs, 800 nm Ti–sapphire laser pulse, split into two delayed replicas in a Michelson interferometer were focussed in an argon jet yielding two independent harmonic pulses. The resulting XUV intensity was monitored as a function of the delay between the two fundamental pulses and showed (1) a periodic modulation of the XUV signal with a period of 1.3 fs and (2) a single 50 as feature prominent at the beginning of the trace. Considering this result as a simple linear superposition of two XUV replicas of the same pulse, as stated before, the only information that can be retrieved is the power spectrum of the radiation. The modulation at $2\pi/\omega_{\mathrm{L}}$ reflects the fact that harmonics are $2\omega_{\mathrm{L}}$ apart in frequency, while the attosecond feature appears to be the temporal counterpart of a continuous background *assumed* to have the suitable spectral phase distribution, which unfortunately cannot be unequivocally established by this experiment. However, things are even more complicated: the nonlinear interaction, required for an intensity autocorrelation, could be the same nonlinear interaction giving rise to the harmonics inside the argon jet. As correctly pointed out by Corkum (2000), 'because production and measurement are entwined, the measurement is not completely transparent, so the method is controversial' and some controversy did arise (Papadogiannis *et al* 2001, Tempea *et al* 2001) surrounding the interpretation.

3.3.2. Intensity autocorrelation. Although methods based on the determination of the *spectral* amplitude and phase may be dubbed as 'direct', as any time-domain method, it is interesting, when possible, to use autocorrelation methods. The principle is very simple: two replicas of the XUV pulse are focused in a gas whose ionization energy is such that two photons are required to free one electron. The two-photon ionization signal is then proportional to the square of the intensity, as with the second harmonic generation in the visible range. When the two replica pulses are superposed with a delay τ, the resulting ionization signal

is the autocorrelation function $S(\tau) \propto \int I(t-\tau)I(t)\,\mathrm{d}t$. The direct two-photon ionization autocorrelation of an XUV pulse remains difficult and has been demonstrated only in a limited number of cases for femtosecond pulses (Sekikawa *et al* 1999).

For the case of attosecond pulses, a demonstration has been achieved only very recently. Tzallas *et al* (2003) indeed just achieved a few weeks ago (at the time of writing this) what was thought almost impossible up to now, namely a direct autocorrelation measurement of the pulse train resulting from the superposition of several harmonics, as predicted by the theory. In practice, the method was implemented as follows (figure 13): harmonic generation in a xenon gas jet using an annular Ti–sapphire laser beam of 130 fs pulses at a wavelength of 790 nm was used to produce the attosecond pulse train. For the second-order autocorrelation of this harmonic superposition, a wavefront splitting arrangement, consisting of a spherical mirror cut into two halves controlled by a piezo-crystal translation unit, was used. The two parts of the bisected XUV pulse train are brought into a common focus in a helium gas jet that is two-photon ionized. The ions are then detected as a function of the displacement of the two half mirrors. This nonlinear signal is suitable for an intensity autocorrelation measurement, although with a significant background (the contrast is less than 3). Moreover, although the second-order autocorrelation technique provides a 'direct' duration estimate, the result depends on the assumed pulse shape. The result found in that particular experiment is more than twice the Fourier limit, which points to a less efficient phase-locking of the harmonics in the case of xenon as compared with argon (Paul *et al* 2001, Mairesse *et al* 2003). It is likely that the autocorrelation method will remain of limited use in practice due to the weak intensity of the harmonic source.

3.3.3. Two-colour, two-photon ionization: sidebands. The alternative to single-colour, two-photon ionization is a two-colour, two-photon (or multiphoton) ionization process combining the XUV pulse to be characterized and an intense infrared pulse. In the low intensity limit, when only one or two photons from the intense field are absorbed or emitted, lowest-order perturbation theory is sufficient for describing this process. However, we sketch here a more general approach in which the infrared intensity can be high (Cionga *et al* 1993 and references therein). It bridges the gap between the perturbation theory and the classical ansatz to be discussed later on (section 3.5.1). Consider a ground state atom exposed to both high frequency, low intensity (x-ray) and low frequency, intense (IR) pulses. Let $\boldsymbol{A}_{\mathrm{X}}$ and $\boldsymbol{A}_{\mathrm{IR}}$ be the vector potentials of the x-ray and IR fields, respectively. The transition probability induced by the two fields may be written as the S-matrix for a one-photon x-ray transition:

$$S = \mathrm{i}\int \mathrm{d}t\,\langle\phi_k(t)|\frac{\boldsymbol{A}_{\mathrm{X}}\boldsymbol{p}}{c}|\phi_i(t)\rangle \tag{8}$$

where $|\phi_i(t)\rangle$ is the time-dependent wave function of the ground state in the presence of the IR field, which has an adiabatic turn-on, and $|\phi_k(t)\rangle$ is a positive energy electron state of asymptotic momentum $\boldsymbol{k}$ submitted to the IR field and the atomic potential V. Both $|\phi_i(t)\rangle$ and $|\phi_k(t)\rangle$ are solutions of the Schrödinger equation

$$-\mathrm{i}\partial_t|\phi(t)\rangle = \left(\frac{p^2}{2} + V + \frac{\boldsymbol{A}_{\mathrm{IR}}\cdot\boldsymbol{p}}{c}\right)|\phi(t)\rangle. \tag{9}$$

Equation (9) is solved by making the approximations that the ground state is not affected by the IR field and is therefore taken as $|\phi_{\mathrm{g}}\rangle$, while for the continuum state one may ignore the influence of V and use the so-called Volkov exact solution of the Schrödinger equation for a free electron in an electromagnetic field:

$$\chi_{\mathrm{v}}(t) = \exp[-\mathrm{i}\boldsymbol{k}\cdot\alpha(t)]\chi_0(t). \tag{10}$$

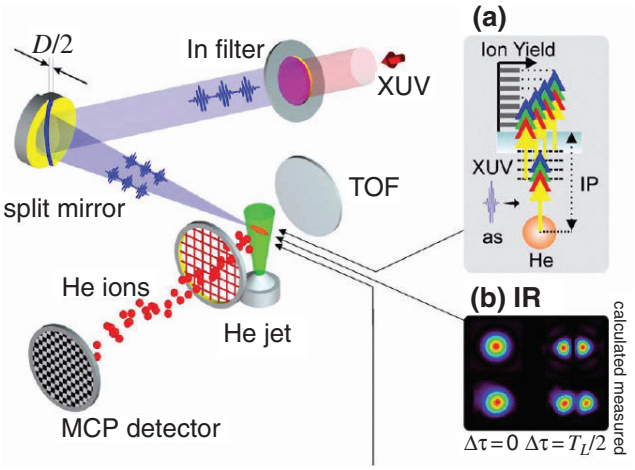

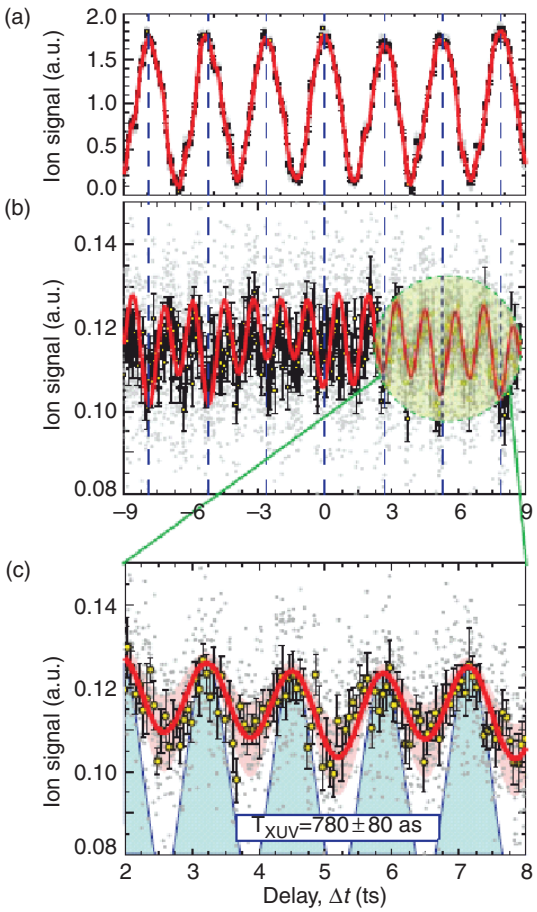

Figure 13. Intensity autocorrelator and autocorrelation traces of an attosecond pulse train produced by harmonics 7–15 generated in xenon measured for the first time. The XUV bursts of the train have a duration of 780 ± 80 as (from Tzallas *et al* (2003)).

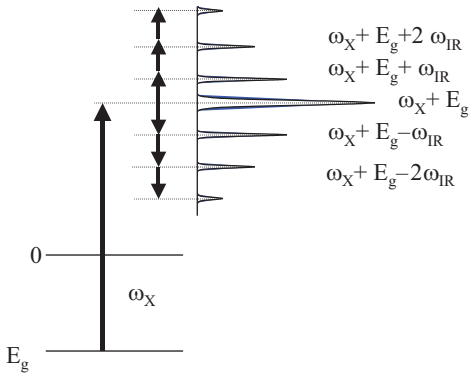

Figure 14. In presence of a strong IR field ($\omega_{\rm IR}$), the photoelectron energy spectrum from the photoionization of an atom ($E_{\rm g}$) by an XUV photon ($\omega_{\rm IR} > E_{\rm g}$) shows sidebands separated by $\omega_{\rm IR}$. They result from two photon transitions in which the XUV photon is absorbed and one or several IR photons are absorbed or emitted.

Here $\alpha(t) = \alpha_0 \sin\omega t$, and $\alpha_0 = E_0/\omega^2$ is the classical oscillation amplitude for an electron in a field E_0 with frequency ω, given in atomic units. The transition matrix element can be written as

$$S = \sum_{n=-\infty}^{\infty} S^{(n)} \delta(E_k - E_{\rm g} - \omega_{\rm X} + n\omega_{\rm IR}) \tag{11}$$

with

$$S^{(n)} = -{\rm i}\pi\, J_n(\boldsymbol{k}_n \cdot \boldsymbol{\alpha}_0) \langle \chi_{\rm v} | \frac{\boldsymbol{A}_{\rm X} \cdot \boldsymbol{p}}{c} | \phi_{\rm g} \rangle \tag{12}$$

in which $J_n(x)$ is the Bessel function of order n and

$$\frac{k_n^2}{2} = E_{\rm g} + \omega_{\rm X} \pm n\omega_{\rm IR} \tag{13}$$

is the kinetic energy of the outgoing electron (for a more exact treatment, see Cionga *et al* (1993)). The physical interpretation of the S-matrix amplitudes is quite clear. The electron is excited into the continuum by the x-ray photon, where it can emit or absorb n-photons from the IR field. From equation (11), the photoelectron energy spectrum will consist of a double series of lines separated by the IR photon energies, on both sides of the primary photoionization peak produced by the XUV photon alone (figure 14). In the low intensity limit, the first sideband amplitude may be used as a cross-correlation signal (Schins *et al* 1994, Glover *et al* 1996) for femtosecond pulses since it is proportional to the convolution of the XUV and infrared pulses. However, this method is hardly useful for attosecond pulses since the IR pulse with which they would be intensity-correlated is much longer (a few femtoseconds in the best case), while in the femtosecond domain it is the infrared intensity averaged over the XUV pulse profile that determines the *amplitude* of the sidebands. However, for the attosecond case, the XUV pulse is shorter than the infrared optical half-cycle, and the only option is to use the electric field as a clock. This is better understood when using the classical ansatz, described in section 3.5.1.

3.3.4. FROG and SPIDER characterization of high harmonic pulses. FROG (Trebino *et al* 1997) is one popular method of complete characterization of femtosecond, visible pulses. It can be extended to XUV femtosecond pulses (Norin *et al* 2002, Sekikawa *et al* 2002) by using two-photon ionization as a nonlinear device, at least for low-order harmonics. The

SPIDER method of Iaconis and Walmsley (1999), based on the spectral interferometry of Froehly *et al* (1973), is one of the most efficient ways of obtaining a complete characterization of an ultra-short pulse. Two replicas of the unknown pulse are delayed in time by τ and frequency-sheared through sum-frequency generation with two different frequencies provided by a third chirped pulse. The resulting summed spectrum displays fringes with a period $\propto 1/\tau$, from which the unknown pulse can be characterized completely in the time domain through an algebraic (i.e. involving a finite number of steps) algorithm. The extension of the SPIDER method to the XUV domain (Muller 2002) is not obvious. First, producing replicas is difficult since XUV beam splitters are not easily available (although we will see that some solutions to this problem can be envisioned). Second, all nonlinear material are strongly absorbing at short wavelengths. Consequently, two-colour, two-photon atomic ionization must be used and the photon's frequency spectrum transferred to the photoelectron energy spectrum. In SPIDER, τ is chosen large enough so that the Fourier transform of the interfering part is well separated from the noninterfering components, enabling easy spectral filtering. Conversely, τ must be small enough for the spectrometer to resolve the fringes. Substituting an electron spectrometer for an optical spectrometer raises issues concerning adequate resolution and places additional constraints on τ. Measuring the spectral amplitudes and phases is strictly equivalent to measuring the field variations of an unknown pulse in the time domain (which, in this case, is obviously unaccessible).

3.3.5. RABITT characterization: two-photon, three colour ionization. The reconstruction of attosecond beating by interference of two-photon transition (RABITT) method described below can be viewed as a SPIDER in which the up-conversion is accomplished by two-photon, three-colour ionization with $\tau = 0$. Moreover, in order to remove the phase ambiguity introduced by the latter condition, the measurement must be repeated, and therefore the method is not single-shot (Muller 2002). Otherwise, it is well adapted to a kind of spectrum that is the only one identified to be fatal to SPIDER, namely a series of equidistant narrow lines produced by a long fundamental pulse[7].

Assuming the theory (Antoine *et al* 1996) in section 2.3.2 is correct, harmonics from a macroscopic medium should be phase-locked, at least under certain conditions. In order to verify this prediction, the phase relation between adjacent harmonics contributing to the XUV bursts must be determined. This reduces to the problem of ionizing an atom by two harmonics of consecutive orders, $\omega_{q-1} = (q-1)\omega_{\mathrm{L}}$ and $\omega_{q+1} = (q+1)\omega_{\mathrm{L}}$, in the presence of the fundamental IR field, ω_{L}. Véniard *et al* (1996) proposed a solution by generalizing the case described in section 3.3.3 such that the IR intensity is sufficiently low for each harmonic to have only one sideband on either side of the primary XUV continuum transition. The photoelectron energy spectra will thus contain five peaks: the two peaks caused by the two harmonics and three sidebands caused by two-photon ionization (figure 15). The central peak corresponds to a quantum state that can be reached through two indistinguishable paths. From Fermi's Golden Rule, the total transition probability from the initial state $|\psi_i\rangle$ with energy E_0 to a final state $|\psi_f\rangle$ (f is the angular quantum number of the continuum electron) at the central sideband with energy $E_q = E_0 + q\omega_{\mathrm{L}}$ is proportional to

$$S = \sum_f \left| M^{(+)}_{f,q-1} + M^{(-)}_{f,q-1)} \right|^2 \tag{14}$$

with

$$M^{(\pm)}_{f,q} = \langle \psi_f | D^{\pm}_{\mathrm{IR}} (E_q - H)^{-1} D^{+}_{q} + D^{+}_{q} (E_{\pm} - H)^{-1} D^{\pm}_{\mathrm{IR}} | \psi_i \rangle \tag{15}$$

[7] The SPIDER technique is very difficult or impossible to use for characterizing a pulse train since it requires that the shear be less than the linewidth of a *single* harmonic order to produce an interference pattern.

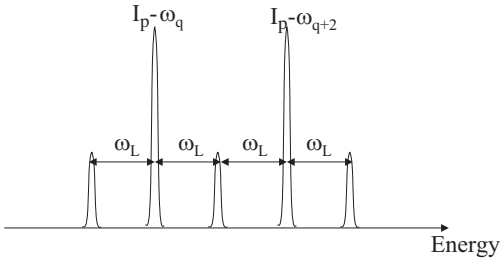

Figure 15. Photoelectron energy spectrum corresponding to a three-colour ionization: two consecutive harmonics and the fundamental. The middle sideband is shared by the two harmonics.

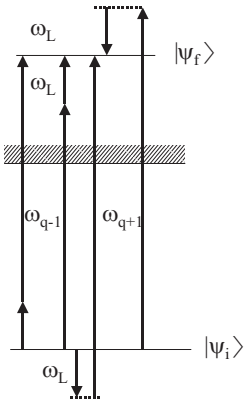

Figure 16. The energy level diagram of the RABITT method. The four transitions leading from the initial $|i\rangle$ to the final $|f\rangle$ states involve one or the other harmonic and differ by the order in which the photons are absorbed or emitted. The total transition probability is obtained by summing and squaring the corresponding four amplitudes.

in which $D^{\pm}$ are the dipole operators that raise or lower the energy, respectively (see figure 16):

$$E(t) \cdot r = D^{+} \exp[-\mathrm{i}\omega_{\mathrm{L}} t] + D^{-} \exp[+\mathrm{i}\omega_{\mathrm{L}} t]. \tag{16}$$

Because one path involves the emission and the other the absorption of one laser photon, they have opposite phases. Explicitly writing the dipole operator phases $D^{\pm} = D_0 \exp^{\pm \mathrm{i}\varphi}$, the interference term in equation (14) becomes

$$A_f \cos(2\varphi_{\mathrm{L}} + \varphi_{q-1} - \varphi_{q+1}) + \Delta\varphi^{f}_{(\mathrm{atomic})} \tag{17}$$

where $A_f = 2|M^{(+)}_{f,q-1}||M^{(-)}_{f,q+1}|$. Delaying the IR laser field by a time τ with respect to the harmonic fields sets $\varphi_{\mathrm{L}} = \omega_{\mathrm{L}}\tau$. Second-order perturbation theory predicts that the amplitude of the sideband common to both harmonics will be modulated by the cosine function in equation (17) with a period equal to half that of the IR laser when τ is varied. This is of course reminiscent of the classical modulation of the photoelectron energy in the high intensity limit. Recording this variation therefore gives access to the harmonics phase difference, $\varphi_{q-1} - \varphi_{q+1}$. The extra phase, $\Delta\varphi^{f}_{(\mathrm{atomic})}$, in equation (17) is the intrinsic phase of the matrix elements for above-threshold, two-photon ionization, which involves a resonance in the continuum and hence an integral leading to a real principal part and an imaginary δ-function. This phase can be calculated with high precision (Toma and Muller 2002), at least for a suitable choice of the target atom.

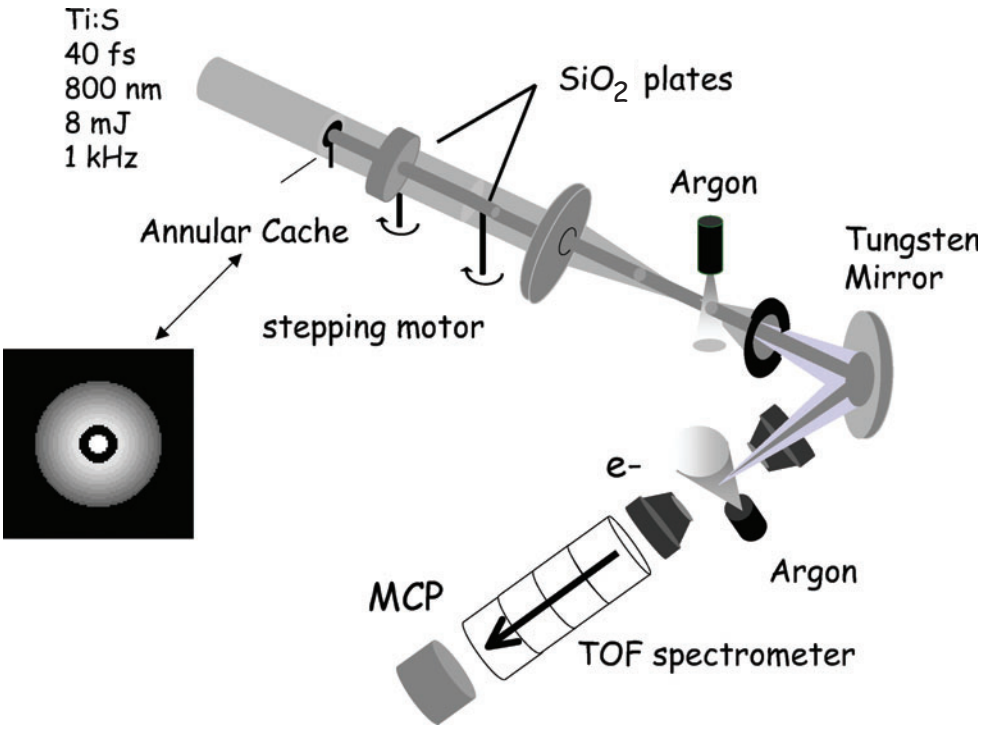

Figure 17. The RABITT set-up. The annular cache separates the input beam in two concentric beams. The two plates control the relative phase (delay with attosecond resolution) of the pulse that generates the harmonics and the one, used to ionize the second jet together with the harmonics generated in the first one (from Paul *et al* (2001)).

3.3.6. RABITT set-up and results. The principles discussed above have been implemented by Paul *et al* (2001). The pump pulse from a 40 fs, 800 nm Ti–sapphire laser is split into two collinear, co-axial beams by a disc (6–10 mm diameter) with a central pinhole (1–2 mm diameter). (This is a variant of the annular beam method, first proposed by Peatross *et al* (1994).) The external annular beam was focused in an argon jet to generate harmonics and subsequently blocked by a pinhole optically conjugated to the disc. The central fundamental beam and the harmonics of orders 11–19 were focused by a spherical tungsten-coated mirror into a second argon jet, producing photoionization. The mirror's reflectivity limited the maximum harmonic order to 19. The photoelectrons were analysed in a time-of-flight electron spectrometer as the delay between the two pulses was scanned by stepping the angle of a glass plate by small increments (a few attoseconds) (see figure 17). The modulation of the sideband amplitude versus delay contains the pairwise phase difference needed to complete the temporal description of the pulse trains. This particular experiment was performed with harmonics generated in the argon 'plateau'. A good modulation depth of a factor of about 2 was observed, showing that the relative phases do not fluctuate much over the beam profile, from shot-to-shot or within the temporal profile of a single pulse. Figure 18 shows that the curves oscillate almost in phase, with a periodicity of 1.35 fs, i.e. half of the IR field period, as expected. From the fitted pairwise phase differences, the phases of the harmonics are found to follow approximately a linear scaling. Together with the relative harmonic intensities, they determine uniquely the temporal intensity profile of the total field (figure 19), with the following

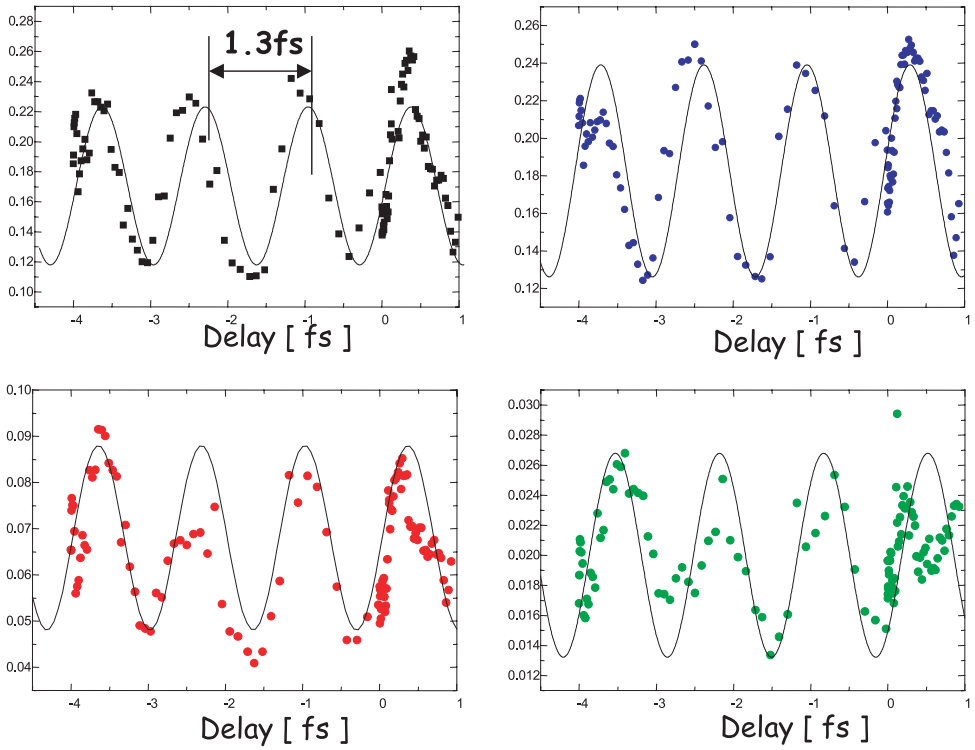

Figure 18. RABITT signals: modulation of the amplitudes of the four sidebands observed when ionizing argon by superposing four harmonics (13–19) of a Ti–sapphire laser (800 nm) and the fundamental. The sine functions are fitted (from Paul *et al* (2001)).

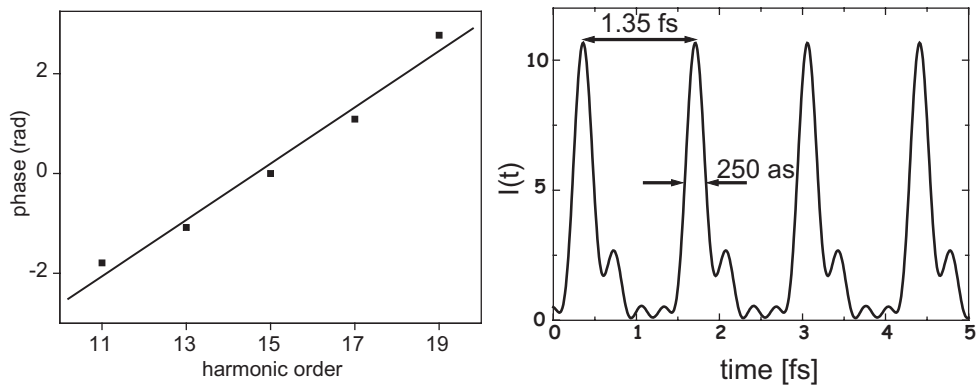

Figure 19. Relative phases (left) and temporal profile of the corresponding pulse train deduced from the data shown in figure 21. The quasi-linear spectral phase determines the shortest pulse measured (250 as). The sideband (18) is slightly off but the accuracy of the measurement did not allow a decision whether this was the beginning of a systematic deviation (from Paul *et al* (2001)).

reservation: the photoionization part of the RABITT method provides information only on the sideband above the target atom ionization threshold. Therefore, it does not reveal the possible influence of harmonics below that threshold whose contribution could modify the temporal profile of the total field. Although numerical solution of the Schrödinger equation indicates

that the harmonics below the threshold are much weaker than a perturbative calculation would predict, conclusions from RABITT are, strictly speaking, valid only for a filtered group of harmonics identical to the ones detected by the spectrometer. The standard deviation of the measurement of Paul *et al* (2001) is about 20 as in the FWHM pulse duration. The linearity of the spectral phase is not perfect, as apparent in figure 19, and involves a small quadratic term that will be commented on later. Provided the IR bandwidth is relatively small, RABITT in principle analyses all individual frequency components within the harmonic bandwidth simultaneously and independently, with each part of the sideband peak responding to the two frequency components that contribute to it. Furthermore, the energy peak profile would show modulations if the phase differences varied over the bandwidth. The experiment showed no such variation, indicating that the harmonics must be frequency modulated (or 'chirped') in a similar way. An identical chirp in all harmonic orders does not affect the intensity envelope of the attosecond pulses but only the phase of their carrier wave. Like other characterization methods, RABITT does not provide information on the absolute phase. Finally, the RABITT method works because we are interested only in the average shape of the XUV field during an optical half-cycle, and therefore it suffices to sample the spectrum at 2ω intervals. This is a consequence of the fact that the XUV emission was very similar from one half-cycle to the other, making this coherent average a meaningful quantity (Muller 2002).

3.4. Limits of attosecond pulses from a group of harmonics

It would be somewhat optimistic to expect that the temporal intensity profile of a large group of N-order harmonics would simply be given as the Fourier limit, $I(t) \propto \sin^2 N\omega t / \sin^2 \omega t$. Although the RABITT measurement of the five harmonic orders, 11–19, generated in argon agrees with this prediction to first approximation, it hints at a long range divergence. The actual result is not Fourier limited, and a close inspection of the harmonic phase versus order reveals a quadratic trend that is confirmed by a least square fit (Kazamias *et al* 2004). This implies a linear dependence of the spectral phase *derivative* that can be assimilated to the emission time of the harmonic in the semi-classical three-step model (section 2.3.1). A linear fit reveals a chirp of about 20 as/eV corresponding to a total time difference over the four harmonics of 236 as of the order of the total duration of the bursts. A recent observation by Mairesse *et al* (2003) over a larger number of orders confirms the trend suggested by the harmonic orders 11–19 and its origin in the different recombination times of the different harmonic orders.

Moreover, the harmonic's spatial phase behaviour must also play a role since any realistic beam has a radially dependent pump intensity and hence a varying dipole phase. A calculation (Gaarde and Schafer 2002) evaluating the degree of phase-locking in argon and neon gases interacting with an intense laser pulse for a range of macroscopic conditions emphasized this spatial phase dependence, which is determined by the interplay between the intrinsic dipole phase and the phase-matching in the nonlinear medium.

3.4.1. Temporal limitation: synchronization of high harmonics. We first examine the theory and ask whether a delay between harmonics orders can be inferred from the three-step model. Each harmonic's complex amplitude is obtained as a sum over all quantum paths, with a phase equal to the quasi-classical action of equation (6). The primary trajectories are those satisfying the classical least action principle, $\delta S = 0$, which are determined by the saddle-point method (not detailed here). Purely classical calculations (Kazamias *et al* 2004) lead to an analytical expression of the chirp, i.e. the variation of the recombination time as a function

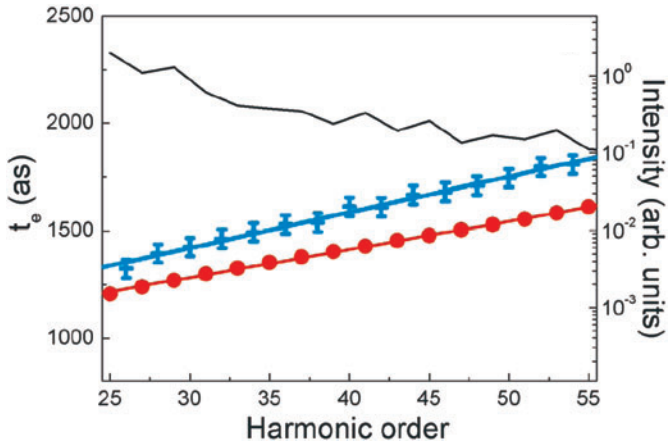

Figure 20. Emission times versus order for harmonics 25–55 generated in neon. Time is clearly not a constant but a linearly *increasing* function of the order. The sign of the slope definitely indicates that the short trajectory is dominant. The experimental (upper curve) result is in excellent agreement with the quantum calculation (lower curve) (from Mairesse *et al* (2003)).

of the harmonic order:

$$C(\Delta E) = \frac{-(t - t')}{\sqrt{8U_p\Delta E}(\sqrt{(\Delta E/2U_p)} + \omega\cos\omega t(t - t'))} \tag{18}$$

where ΔE is the kinetic energy gain in the second of the three steps, ω the laser frequency, U_p the ponderomotive energy and t' the time of the first step.

In Mairesse *et al* (2003), a quantum calculation of the derivative of the spectral phase, equivalent to a group delay in the emission, is shown to be equal to the real part of the complex recombination time associated with the trajectory, resulting in the emission of the corresponding harmonic. The calculation reveals that, over a large range of orders, the emission time varies quasi-linearly with the frequency with a positive slope for the 'short' trajectories and a negative slope for the 'long' ones, which are the main contributions, as discussed in section 2.3.1. Both the classical expression (equation (18)) and quantum calculations are in good agreement with the experiment and confirm that only one trajectory (the 'short' one) contributes to the harmonic generation. The constant delay from one order to the next is found to vary as ω_1/U_p, where ω_1 is the fundamental frequency.

Experimental measurements (Mairesse *et al* 2003) were performed under conditions similar to those of Paul *et al* (2001), except that a larger range of harmonic order ($\leqslant$23) was monitored. To this end, a broadband, grazing-incidence Pt toroidal mirror replaced the tungsten-coated mirror, which limited the harmonics energy to 30 eV. A clear deviation from the linear phase was found (figure 20): the spectral phase is quadratic as a function of the order, while its derivative, $\partial\Phi/\partial q = aq + b$, is linear. The slope of the function $\partial\Phi/\partial q$ is found to be 106 ± 8 as for one order to the next. It is the time lag between the emission times of the successive orders. This value agrees with the 30 as eV^{-1} deduced from equation (18) for an intensity of 10^{14} W cm^{-2}. Moreover, the sign of the chirp confirms experimentally the importance of the 'short' trajectory.

Mairesse *et al* (2003) established this trend firmly by measuring the phase difference over 30 consecutive harmonic orders (11–69) generated in neon, thus allowing the reconstruction of the harmonic emission profile with a 50 as resolution. The result establishes accurately a delay of 33 ± 3 as per order (to be compared with the calculated value of 26.1 ± 0.2 as) (figure 21).

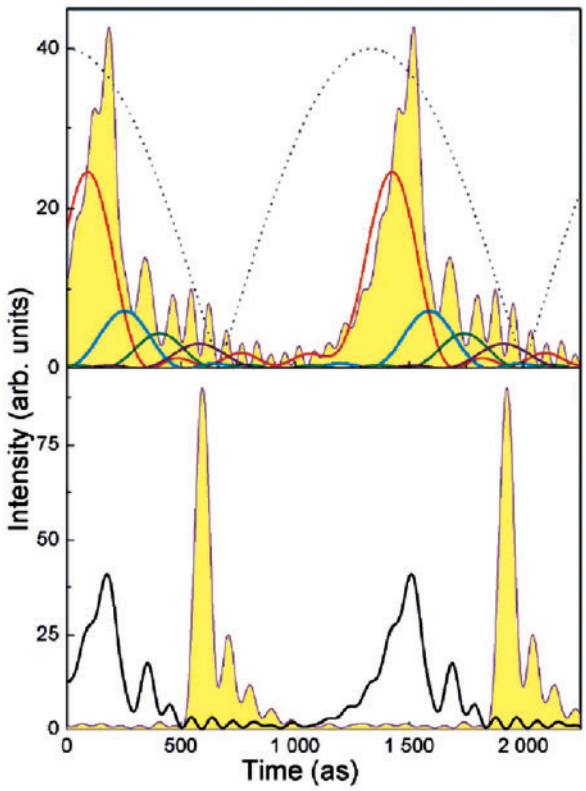

Figure 21. The shortest possible pulse is not obtained by superposing more harmonics: each harmonic is actually delayed by a time depending on its order and leading to the temporal profile shown by the filled curve in the upper box. Grouping the harmonics by 5 clearly shows this increasing delay. The shortest pulse is actually obtained by limiting the number of summed harmonics. Here summing 25 harmonics yields 150 as pulses, three times the Fourier limit. while filtering only 10 harmonics yields 130 as pulses, close to the Fourier limit. This minimum pulse can be further compressed (filled curve in the lower box) by propagation in a negative dispersion medium (see text) (from Mairesse *et al* (2003)).

Both the theoretical analysis and the RABITT measurements show that low-order harmonics are emitted close to the peak of the field in the pump's optical cycle, while high-order ones are emitted close to the zero-crossing point. This time lag constitutes a fundamental limit for synthesizing attosecond pulses from high harmonics. Thus, for 22 (25–69) consecutive harmonic orders, the limit (150 as) is three times the Fourier transform, while it can be lowered to 130 as, i.e. about the Fourier limit, by limiting the spectral range to 11 orders. The shortest pulse does not correspond to the broadest bandwidth but to an optimal number of harmonic orders.

Note that, as the time delay scales as ω_1^3, it would be possibly advantageous to use mid-infrared lasers (Sheehy *et al* 1999). Note also that, in principle, the temporal delay could be compensated by propagating the harmonics in a medium with negative group velocity dispersion (where low frequencies travel faster than high ones). For instance, propagation through a fully ionized plasma could compress the 127 as pulse to 75 as (i.e. 3 atomic units). One last remark: this analysis also holds for single attosecond bursts produced by few-cycle pulses (Drescher *et al* 2002) (see below).

3.4.2. Spatial variation of the intrinsic phase. The previous conclusions are based on the calculated single atom response. The macroscopic aspects of the spatio-temporal behaviour of the dipole phase have been addressed by Gaarde and Schafer (2002) by direct numerical integration of the time-dependent Schrödinger equation and subsequent solving of the Maxwell wave equation in the slowly varying envelope approximation. The model also includes the three-dimensional distribution of the pump laser intensity and the relative position of the jet with respect to the focal distribution. Conditions similar to those used by Paul *et al* (2001) for argon, as well as the extension to the superposition of larger numbers of harmonics in neon, were simulated. The radial profile of each harmonic at the exit of the medium, is calculated. At a given time, t_0, during the pulse, the time profile of the emission from the combination of odd harmonic orders n through m is then constructed as an average over the radial distribution of the harmonic fields:

$$I_{\mathrm{X}}(t, t') = \int r \, \mathrm{d}r \left| \sum_{q=n}^{m} E_q(r, t') \mathrm{e}^{-\mathrm{i}[q\omega_1 t - \phi_q(r,t')]} \right|^2 . \tag{19}$$

Here t' is the time during the pulse profile, while t refers to the rapid variations of the field within one cycle and r is the radial coordinate. The time profile of equation (19) differs from equation (3) in Antoine *et al* (1996) as it includes the spatial variation of the phase with intensity. Confirming the findings of Antoine *et al* (1996), the phase-locking is found to depend on the macroscopic conditions (namely the position, z_0, of the atomic gas jet with respect to the pump's focus, characterized by a Rayleigh range $b/2$). The results indicate that there are generic macroscopic conditions that, in general, lead to good phase-locking. In particular, good phase-locking can be achieved over a range of z_0 close to $-b/2$, i.e. when the laser is focused approximately one Rayleigh length before the centre of the gas jet. Not surprisingly, this situation corresponds to the best on-axis phase-matching conditions, where the phase variation of the nonlinear polarization over the medium length is minimal (Salières *et al* 1995).

By defining a radially averaged phase difference, $\overline{\Delta\Phi_{q+1}}$, between neighbouring harmonics q and $q+2$, an approximately constant time lag is found, in agreement with the quasi-classical calculation and the experiment described in the previous section. Even for the case of a constant average phase difference, $\overline{\Delta\Phi_q}$, the *spatial* distortion of the harmonic wave fronts can have a profound effect on the attosecond pulse train structure. A simple example of this is given by Gaarde and Schafer (2002): the superposition of harmonics with constant phases and only pairwise spatial overlap would still yield the same type of signal as measured by Paul *et al* (2001); however, the lack of spatial overlap between all the harmonics would give rise to very broad peaks in the time profile. However, usually, on-axis harmonic emission is selected by a small pinhole at the entrance of the spectrometer. The optimization procedure of the harmonic flux then selects naturally the best macroscopic conditions for the phase-locking and guarantees that all the harmonics are actually superposed in the far field, an obviously necessary condition for the generation of attosecond pulses.

3.5. Single attosecond pulse

The other route to attosecond pulses relies on high harmonics generated by an ultra-short (few-cycle) pump pulse. Chirped-pulse amplified Ti–sapphire laser systems are able to generate 5–10 fs pulses at the millijoule energy levels. These pulses have been shown to generate relatively efficiently harmonics in the 90–100 eV spectral range (Brabec and Krausz 2000). If the selected harmonic spectral range is in the cutoff region, then a simple spectral filtering allows the selection of a single pulse in the time domain since only the highest intensity

part of the pump pulse is able to provide enough kinetic energy to the electron (see figure 23 and the discussion below). To characterize such pulses, the autocorrelation methods described in the previous section must be ruled out, unfortunately, and cross-correlation methods must be used. Intensity cross-correlation (Schins *et al* 1994, Glover *et al* 1996), on the one hand, and ponderomotive streaking of the ionization potential (Toma *et al* 2000), on the other hand, have been implemented. Both are based on photoionization of a target atom in the presence of an intense low frequency electromagnetic field (in practice the infrared pump field). In the streaking of the ionization potential, the effect of the infrared intensity is observed on the photoelectron spectral *profile* since the atom's binding energy increases by the ponderomotive energy and therefore depends on time, i.e. it is 'streaked' during the rising or falling edges of the IR pulse. It results in a broadening of the photoelectron energy spectrum and the measure of this broadening along with the knowledge of the rise time yields the x-ray pulse duration. This technique is limited to pulses at least one cycle long (the ponderomotive shift is the cycle-averaged kinetic energy of a free electron on average at rest in the field and therefore requires at least one cycle to be meaningful). It does provide more resolution than the intensity cross-correlation of the two pulses but is still too slow for attoseconds. All methods must be adapted to access the sub-femtosecond range (early proposals can be found in Constant *et al* (1997)). There are several levels of description of this type of process: a two-colour, multiphoton ionization transition in which the photoelectron changes its energy by absorbing/emitting quanta from the low frequency field. The corresponding signatures are the sidebands in the photoelectron energy spectra discussed in section 3.3.3. However, for sub-femtosecond pulses, the photoelectron energy spectra are broadened to the point where the sidebands, separated by the infrared photon energy, can no longer be resolved. The simpleman's description below often results in an adequate description.

3.5.1. Classical ansatz: simpleman's theory of two-colour ionization. This ansatz consists of separating the process into a photoionization step and a classical motion in the electromagnetic field.

If a single attosecond XUV pulse ionizes an atom during a time much shorter than the external infrared field, the probability of producing a photoelectron is well localized in time. It is moreover assumed that the ionization process itself is independent of the infrared field. We therefore consider a free electron dropped at instant t_i in an electromagnetic field described by a vector potential $\boldsymbol{A}(t)$ with an initial velocity $\boldsymbol{v}_0$. Using atomic units, the canonical momentum conservation requires that

$$\boldsymbol{v}(t) + \boldsymbol{A}(t) = \boldsymbol{v}_0 + \boldsymbol{A}(t_i) \tag{20}$$

or, in terms of the field $\boldsymbol{E}(t) = -\partial \boldsymbol{A}(t)/\partial t$,

$$\boldsymbol{v}(t) + \frac{\boldsymbol{E}(t)}{\omega} = \boldsymbol{v}_0 + \frac{\boldsymbol{E}(t_i)}{\omega}. \tag{21}$$

In the simple case of a linear polarization along the x-axis and an initial velocity $\boldsymbol{v}_0$ making an angle θ_i with the x-axis, the average final kinetic energy, U_f (after the pulse is off), is

$$U_f = U_0 + 2U_\mathrm{p}\cos^2\phi_i + \sqrt{8U_0U_\mathrm{p}}\cos\theta_i\cos\phi_i \tag{22}$$

while the following relationship between θ_f and θ_i is apparent from figure 22 and is given as

$$\tan\theta_f = \frac{v_0\sin\theta_i}{v_f\cos\theta_i + E/\omega}. \tag{23}$$

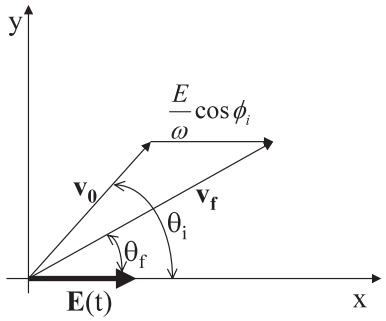

Figure 22. Momentum change imposed on a free electron by the electromagnetic field (the magnetic force is ignored). The initial velocity makes an angle θ_i with the electric field oscillating along x. The electron acquires a drift velocity parallel to E and depending on the initial phase F_i so that its final velocity makes the angle q_f with the field direction. The new velocity results from the canonical momentum conservation.

The final velocity, $\boldsymbol{v}_f$, is given by the sum of the initial velocity, $\boldsymbol{v}_0$, and the drift velocity $\boldsymbol{v}_\mathrm{d} = E(t_i)/\omega$ parallel to the polarization direction. It can be shown (Itatani *et al* 2002) that the final kinetic energy, U_f, is ($\phi_i = \omega t_i$)

$$U_f = U_0 + 2U_\mathrm{p}\cos 2\theta_i \sin^2\phi_i \pm \alpha\sqrt{8U_0U_\mathrm{p}}\cos\theta_i \sin\phi_i \tag{24}$$

where

$$\alpha = \sqrt{1 - \left(\frac{2U_\mathrm{p}}{U_0}\right)\sin^2\theta_i \sin^2\phi_i}. \tag{25}$$

Several proposals for attosecond measurements are based on this approach (see, for instance Quéré *et al* (2003)).

3.5.2. Experimental evidence of a single attosecond pulse. The generation of a single attosecond pulse from high harmonics pumped by a few-cycle pulse, although long predicted by calculation verification, waited for a clear experimental signature. A few milestone experiments (Drescher *et al* 2001) from the Vienna group have paved the way to the experiment to be described below (Hentschel *et al* 2001). The principle of the generation is sketched in figure 23 along with the set-up used for the characterization. First, a few-cycle 800 nm pulse generates high harmonics in a neon jet and produces a train of pulses. The crucial element there (besides the few-cycle intense pump pulse) is the filter, which isolates the spectral content close to the harmonic cutoff and, as a consequence, limits the temporal emission. Each short XUV flash covers a range of frequencies. The highest photon energies near the cutoff are generated only at the highest intensity part of the pump pulse. The calculation predicts that only a single burst of harmonics will be emitted with energies near the cutoff and being temporally confined to the maximum intensity of one-half of an optical cycle. Hence a *spectral* filter (the multilayer shown in figure 23) selects this pulse *temporally*. As shown in figure 23, the x-ray pulse is focused in a krypton jet along with a reduced-intensity infrared pulse by a composite Mo/Si multilayer mirror.

The electrons resulting from the photoionization in the presence of the IR pulse are energy analysed as a function of a delay that is finely stepped by a PZT-controlled mirror. The resulting modulation, shown in figure 24, is in good agreement with the theory: from equation (24) one can see that the kinetic energy of a photoelectron produced by an x-ray pulse shorter than the IR half-cycle depends on the initial phase, ϕ_i. In particular, for a detection angle $\theta_i \approx \pi/2$,

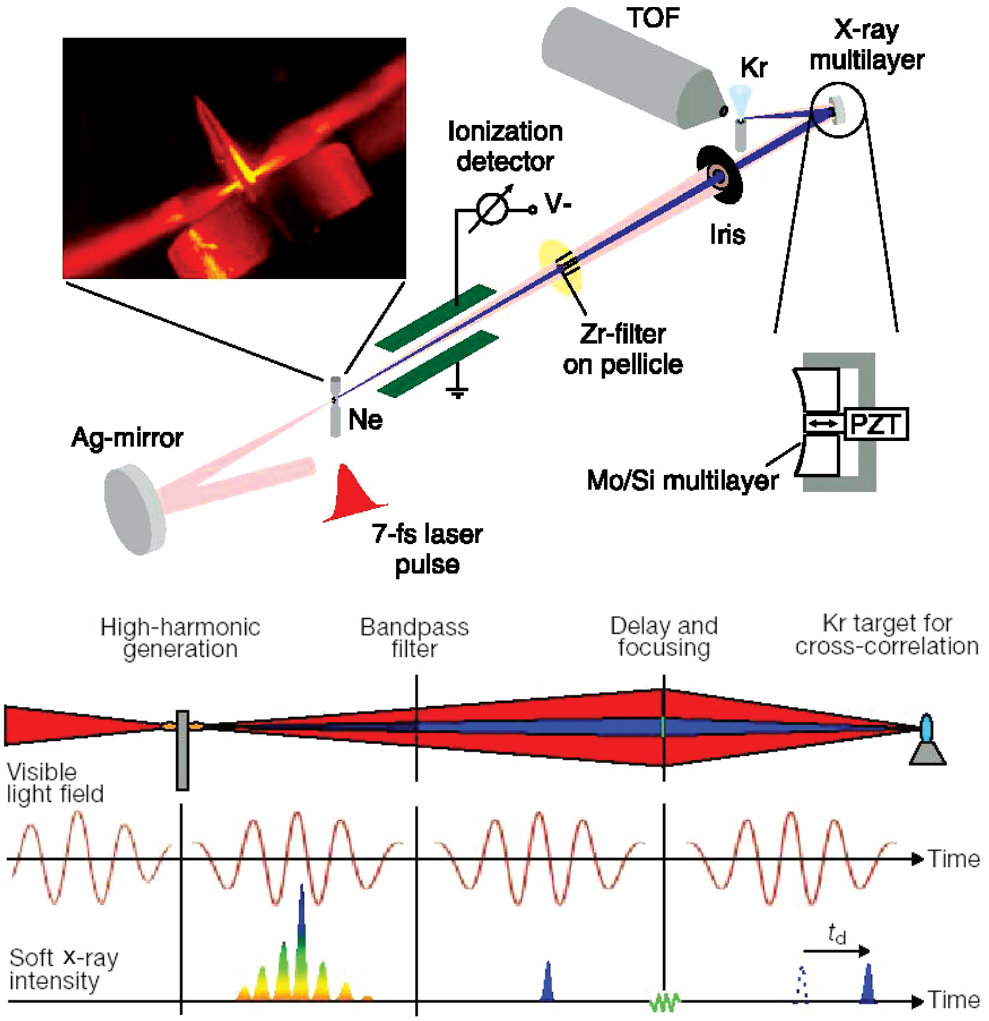

Figure 23. The upper left part shows the set-up used by the Vienna group. High harmonics are generated in neon by a very short (7 fs) 800 nm pulse from a Ti–sapphire laser. A Zr spectral filter eliminates all but the highest frequency harmonics as shown in the lower right part. Since these harmonics are emitted only during a very short part (the most intense) of the pulse, the Zr also acts as a temporal filter. The iris eliminates most of the fundamental laser beam. A small IR beam and the harmonic selected by the Zr are focused on a krypton jet by a multilayer composite spherical mirror whose centre may be displaced by a PZT thus controlling the relative delay between the two pulses. The ionization electron energy spectrum can be thought of as resulting from a two-photon process (see figure 13) or from the momentum change imposed by the field on the photoelectrons (see figure 14). Since the sidebands can no longer be resolved in the experiment due to the sub-femtosecond duration of the harmonic pulse, the second interpretation is used to calculate the broadening of the photoelectron spectrum (from Drescher *et al* (2001)).

the last term in equation (24) is zero, and the energy is simply given by $U_p \sin^2 \phi_i$ and is hence modulated at twice the IR frequency as the initial phase is varied. By monitoring the change in the photoelectron's average kinetic energy detected at 90° from the IR laser polarization, Drescher *et al* (2001) and Hentschel *et al* (2001) could eliminate the drift energy and measure only the dependence of the average oscillation energy on the initial phase (see equation (22)).

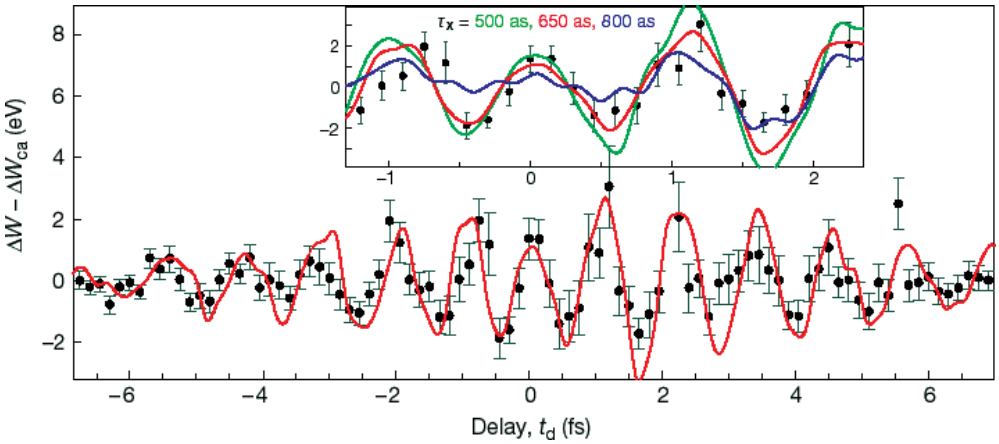

Figure 24. The broadening of the spectrum is an oscillating function of the delay with twice the optical frequency (lower curve) or a 1.35 fs period. The contrast is strongly dependent on the temporal width of the harmonic pulse. The inset shows how the latter can be determined by fitting the observation with calculated functions with different duration. The best fit in this case is 650 as (from Drescher *et al* (2001)).

At first glance, it may seem surprising that a cycle-average energy contains information about the phase, but a simple inspection of the free electron equation of motion shows that its velocity contains three terms: the oscillation velocity, which leads to the ponderomotive energy and is actually stopped when the pulse turns off; a drift velocity depending on the initial phase; and the initial velocity, which gives rise to the crossed-term average energy and also depends on the initial phase. Drescher *et al* (2001) recognized that this last term can be cancelled by detecting the electrons in a direction perpendicular to the laser polarization. Following the classical treatment of Drescher *et al* (2001) (a full quantum calculation has been carried out by Kitzler *et al* (2002)), the visibility of this modulation is expected to reduce as the x-ray pulse length increases and vanishes as it reaches a full half-cycle. For comparison, the kinetic energy observed along the laser polarization ($\theta = 0$) would include both a modulation at ϕ_i and $2\phi_i$ near the initial (rather large) kinetic energy, U_0, and would therefore be more difficult to detect. Fitting the contrast with different pulse lengths yields a value of 650 as, in good agreement with the predicted value of 530 as. This study yields the first evidence of a single attosecond pulse (in contrast to the pulse *trains* discussed in the previous section). In fact, this conclusion cannot be drawn from just the modulation of figure 24. The analysis would yield an identical results if two or several short bursts, instead of just one, separated by half the IR optical period, were present. The evidence of a single attosecond pulse is actually derived from (a) the result of figure 24, (b) comparison with the calculation shown in figure 25 and (c) the observed blue-shift of the IR laser frequency caused by the rapidly varying refractive index induced by the ionization in the harmonic jet. The ensemble provides convincing evidence for the *single* pulse conclusion.

3.5.3. Carrier-to-envelope phase control. Attosecond pulse generation using few-cycle pump pulses faces a unique difficulty, namely the carrier-envelope (CE) phase fluctuations. This phase, which is normally ignored, becomes crucial in the case of nonlinear processes since it depends on the amplitude of the electric field (Cormier and Lambropoulos 1998, de Bohan *et al* 1998, Tempea *et al* 2001). Controlling the CE phase has been achieved by several groups

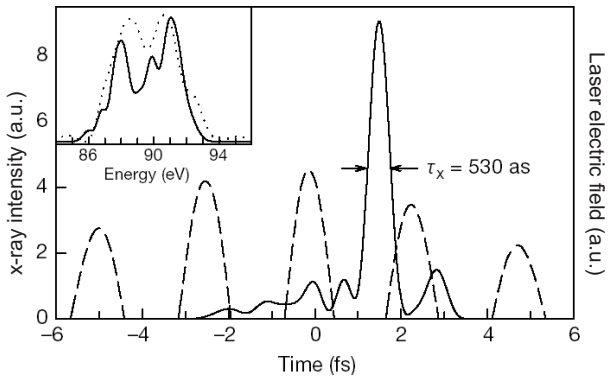

Figure 25. Calculation showing the spectrum (inset) and temporal profile of the couple of harmonics selected by the Zr filter around 90 eV. Given the short envelope profile the sidebands are no longer resolved. The profile indicates a duration of 530 as, in agreement with the measurement (see figure 24) (from Mairesse *et al* (2003)).

(Apolonski *et al* 2000, Jones *et al* 2000, Baltuška *et al* 2003) using the so-called f-to-$2f$ interferometry. The phase-stabilization works by broadening the pulse by a full octave and then detecting the beat frequency between the frequency-doubled and the spectrally-broadened components. The technique is delicate and requires state-of-the-art equipment. The current best result for an amplified system (Baltuška *et al* 2003) is a jitter of less than 50 mrad on the CE phase (root-mean square), corresponding to a remarkable stability ($<1\%$ rms) of the amplified pulse energy. An alternate approach that eliminates the need for the cumbersome rf-circuitry has been discussed by Baltuška *et al* (2002). In this approach, a noncollinear optical parametric amplifier driven by a pump and signal beam derived from the same coherent source is used to generate an idler pulse. The essential feature is that although the CE of the pump and signal pulses are not fixed shot-to-shot, the CE phase of their difference frequency (idler) is constant and controllable.

Applications of this technique to metrology (Jones *et al* 2000) and harmonic generation (Baltuška *et al* 2003) have opened exciting avenues. It is now possible to control efficiently the motion of electronic wave packets. In certain cases, the difficult CE phase control can be circumvented and replaced by single-shot measurements of a well stabilized laser (Nisoli *et al* 2003). Kienberger *et al* (2004) have demonstrated recently that the CE phase control allows the generation, together with the measurement, of single 250 as pulses. The principle of the measurement is the same as above, with the difference that this time the CE phase is controlled accurately. Figure 26 shows the photoelectron energy spectra corresponding to different values of the CE phase. These spectra display both accelerated and decelerated electrons, depending on the phase of the infrared field and provide the proof of single XUV pulses (93 eV) as short as 250 as, the shortest single pulse to date. It is easily predictable that the phase-controlled Ti–sapphire system used in this experiment will become the standard in the near future.

4. Applications

Application of attosecond pulses for time-resolved electron spectroscopy is expected to have a broad impact on many areas of science. This represents a very lofty goal but also a formidable challenge. At the time of writing this, a few experimental applications have been demonstrated: inner-shell processes have been monitored directly in the time domain, while the timing of the three-step quasi-classical model with respect to the pump optical cycle has

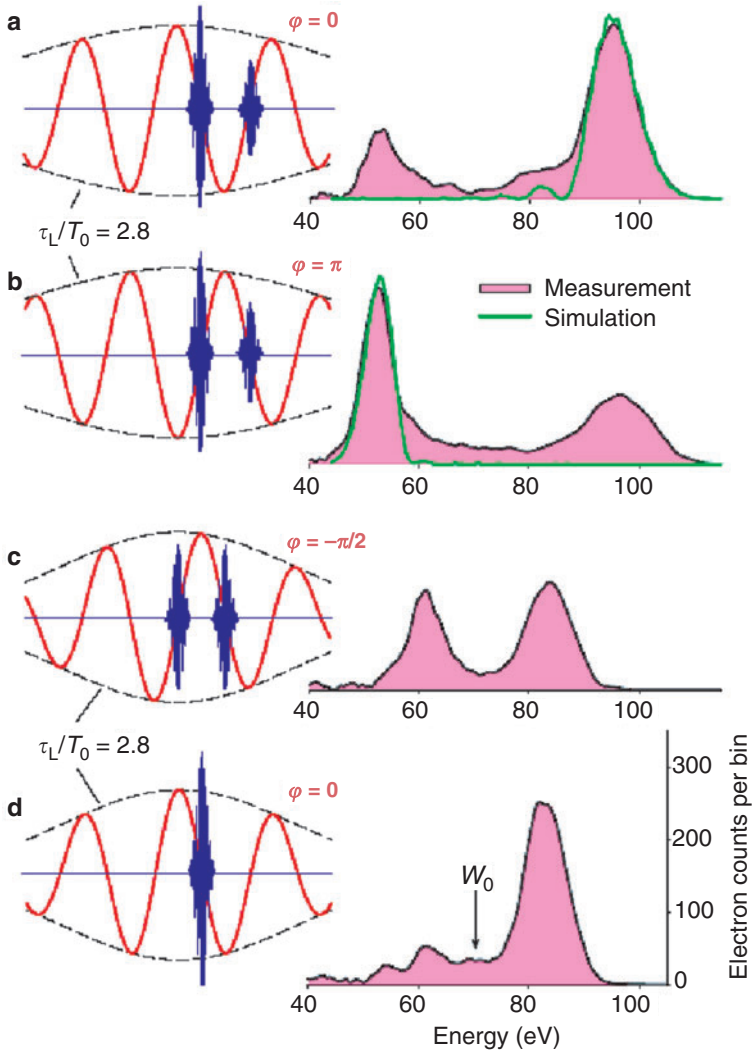

Figure 26. Streaked photoelectron spectra for a fixed delay of the phase-controlled probe laser. In the absence of the probe the spectrum peaks at 72 eV. Energy can be gained or lost in the laser field depending CE phase (φ). The width of the peaks allows one to assign a duration of 250 as to the 93 eV single pulse (from Kienberger *et al* (2004)).

been determined with attosecond precision. Furthermore, many theoretical proposals await experimental verification.

4.1. Time-resolved Auger decay

A breakthrough in observing in real time an inner-shell rearrangement was reported by Drescher *et al* (2002). The experiment is a landmark effort since it is the *first* time that all key elements have been combined in a single attosecond experiment. Referring to figure 27, a 97 eV, 900 as pulse created from a HHG neon source is used to photoionize a 3d electron (process [a]) in krypton in a separate target jet. The photoionization process creates a vacancy in the M-shell (W_h in figure 28), which will undergo an Auger decay: one bound electron fills the hole

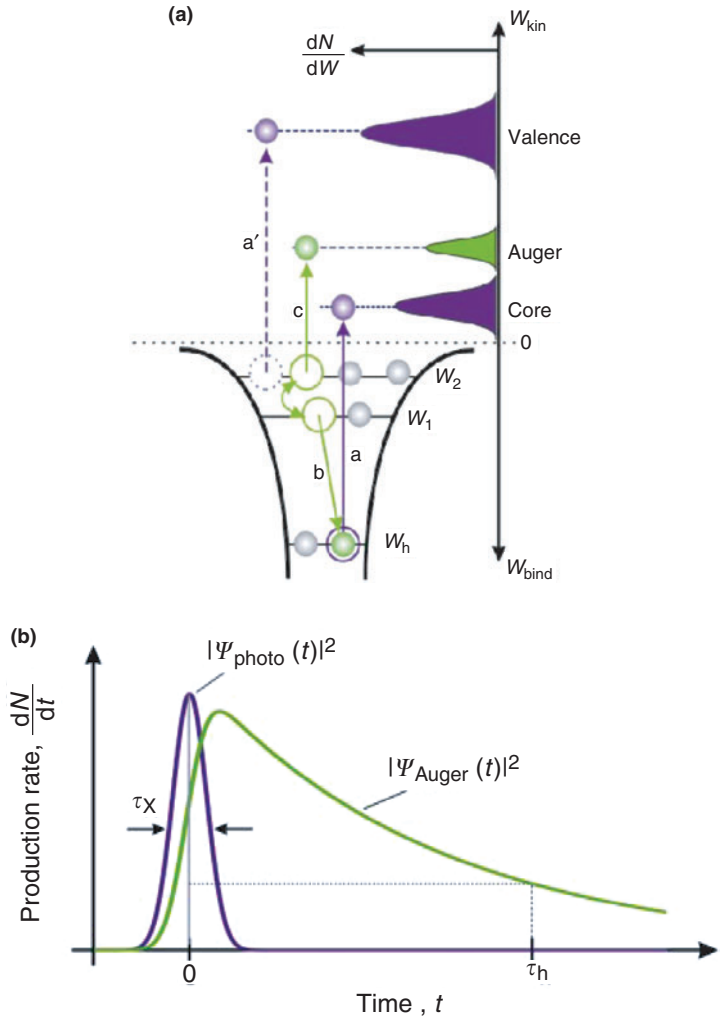

Figure 27. Illustration of the energy levels and relaxation dynamics for an Auger process. The XUV attosecond pulse photoionizes a core electron (energy W_h) along path (a) and results in a temporal signature of the XUV pulse profile shown in plot (*b*). The hole is spontaneously filled by the decay of an electron along path (b) with the simultaneous ionization of a second electron via path (c). The rate of production of the Auger electron is determined by the hole lifetime, τ_h, as shown in plot (*b*). Other processes such as the ionization of a valence electron (see path (a′)) could also occur but can be discriminated by the photoelectron spectrometer (from Drescher *et al* (2002)).

(process [b]), and a second electron is released into the continuum (process [c]). The Auger process is spontaneous and has a corresponding decay lifetime, but the photoemission is prompt and in time would reflect the pulse duration of the 900 as pulse.

The study's aim was to measure in real time the Auger lifetime by monitoring the Auger electron's release time into the continuum after the sub-femtosecond 97 eV photoionizing pulse. The two-colour sideband technique was employed as the detector, but in this case the Auger electron's sideband amplitude was analysed using a photoelectron energy spectrometer. The averaged photoelectron spectrum was recorded as a function of the delay between the

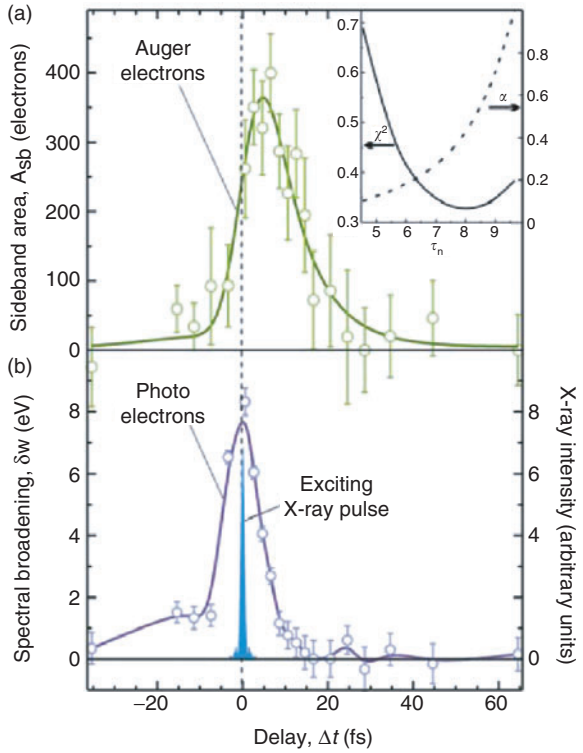

Figure 28. The emission profile of the Auger electron as a function of delay between the XUV and infrared pulses. (*a*) is the sideband area (○) of the Auger line extracted from the photoelectron spectra. The solid line is a fit of an exponential decay convoluted with the pulse profile. Since $\tau_{XUV} \ll \tau_{IR}$, the spectral broadening of the prompt photoelectron emission shown in (*b*) calibrates the response function (from Drescher *et al* (2002)).

97 eV pulse and the intense 5 fs Ti–sapphire pulse. The resulting deconvolution of the data yielded a Auger lifetime of $7.9^{+1.0}_{-0.9}$ fs, which agrees well with the value derived from the frequency domain.

This experiment is significant for a number of reasons. It is the first real time measurement of a fast electronic process and represents the beginning of the attophysics era. Furthermore, it provides a benchmark against a known and independently derived measurement and verifies the efficacy of generating, propagating on target and detection of attosecond pulses. The elegance of the measurement is also evident in the self-referencing provided by the direct photoemission, which allows a check of the metrology against other values.

4.2. Attosecond timing of electron dynamics in HHG

The basic model of HHG (section 2.3.1) involves extraction of the electron via tunnelling, a classical motion under the action of the Lorentz force alone and a recollision with the nucleus in which all the available energy is transformed into a photon. This process is then repeated periodically at each half-cycle, giving rise to the harmonic spectrum of discrete lines separated by 2ω. Theoretically, since the tunnel probability is growing exponentially with the electric field, the electron is ejected close to the field maxima. The field-driven classical trajectories can then return to the origin approximately a half-cycle later. It is naturally interesting to test experimentally the details of this scenario. This could be accomplished easily using the

RABITT method, which determines the timing of the attosecond XUV bursts with respect to the pump cycle in the second atomic jet. It is a matter of evaluating carefully all the phase shifts between the ionization and generation jets to retrieve the interesting timing. Contributing factors include the Gouy phase slip at focus, the dispersion of the gas medium and the metallic reflection at the mirror. All these factors can be evaluated with precision (Dinu *et al* 2003). The attosecond pulses are finally found to occur 190 ± 20 as after each maximum of the fundamental electric field. In the rescattering model, the kinetic energy gain in the continuum is $\Delta E = 2U_p[\sin(\omega t) - \sin(\omega t')]^2$, where U_p is the ponderomotive potential, t' the ionization time and t the recombination time (t and t' are calculated easily). The photon energy is then simply $I_p + \Delta E$. For each harmonic below the cutoff frequency, two trajectories lead to the same photon energy: electrons ionized very early after the peak of the electric field, spending almost one full period in the continuum before recombining ('long' quantum path); electrons ionized slightly later, spending only about half a period in the continuum ('short' quantum path).

For the 15th harmonic (the middle order of the harmonic comb under consideration), the calculation yields a short recombination time of 1380 as and a long one of 2320 as. The earlier propagation time is in excellent agreement with that derived from the experiment (1523 ± 150 as) and excludes the long path. This is a confirmation that the attosecond pulse train arises from the short quantum path. The remarkable efficiency of the semi-classical model is a surprise since argon ionization does not occur in a pure tunnelling regime (Keldysh parameter of 1.14). However, more refined models (Christov *et al* 1997) yield similar timings for the short quantum path, and in a recent numerical study, Gaarde and Schafer (2002) have shown that the phase-locking is highly favoured by the short quantum path, again in excellent agreement with the findings. This study demonstrates that by determining precisely all the phase delays between the harmonic generation point and the detection apparatus, one can measure the timing of the attosecond pulses in HHG with respect to the pump field cycle. This not only yields valuable information on the harmonic generation process by showing that the short quantum path is dominant, in agreement with the theoretical prediction, but is also the first application of an attosecond pulse train produced by superposing on-phase high harmonics for clocking electron dynamics in strong field interaction. The result of Dinu *et al* (2003) was recently extended by Aseyev *et al* (2003) in Kr and Xe in a set-up eliminating the focusing into the ionization zone. Moreover, the set-up, using a velocity mapping detector, yields the angular distribution of the various electron peaks. The new experiments confirmed the robustness of the results and uncovered a remarkable difference between xenon and the other two gases in the timing, attributed to their ionization regimes: while argon and krypton are ionized in the tunnelling regime, xenon is still in the multiphoton regime, where intermediate resonances may affect significantly the recollision time (Muller 2001).

5. Outlook

5.1. High harmonics from scaled atomic interactions

As mentioned earlier, there exists a novel approach to HHG that could provide some insight into attosecond generation, and many of the key elements have already been established. This approach attempts to circumvent the need for novel metrology by using a long wavelength fundamental drive field for generating high harmonic radiation in the visible/near-ultraviolet spectral range. The approach is based on the principle scaling of an intense laser–atom interaction, first discussed by Keldysh (1965). Keldysh proposed that the ionization dynamics can be gauged by considering the ratio of the optical frequency to the tunnel frequency and by doing so equivalent interactions can be realized throughout the electromagnetic spectrum.

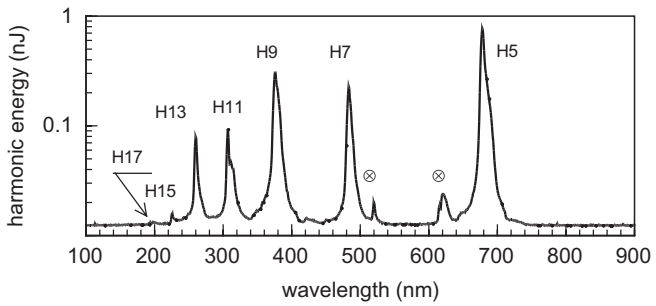

Figure 29. High harmonic spectrum generated by excitation of rubidium atoms with 1.9 ps, 3.6 μm pulses. High harmonics extending to the 17th order are visible while higher orders are beyond the sensitivity of the air-based detection system (<200 nm). This experiment has a comparable interaction energy to xenon atoms exposed to 800 nm pulses. The additional lines in the spectrum can be assigned to fluorescence of Rb. The spectrum is not corrected for the instrumental spectral response (from Sheehy *et al* (1999)).

The interaction of an alkali metal with an intense mid-infrared fulfills this condition and at least qualitatively has been shown to be similar to an inert gas atom exposed to an 800 nm Ti–sapphire pulse.

In these experiments (Sheehy *et al* 1999), a mid-infrared (4 μm) fundamental pulse generates high harmonics from an alkali metal vapour. The evidence for this is shown in figure 29, a comb of harmonics extending to the 17th order is observed and all the emission is confined to wavelengths greater than 200 nm (VUV limit). The cutoff for this process is not observed in the experiment since it should occur at wavelengths shorter (VUV) than detectable by the air optical system. Furthermore, the harmonic energy is sufficient for *direct* temporal characterization using standard metrology, e.g. FROG or SPIDER, and the low-order harmonics pulse duration has been measured using second-harmonic generation autocorrelation (Clatterbuck *et al* 2003, 2004). The measured HHG energies and pulse duration resulted in good agreement with calculations using a 'realistic' single atom response and macroscopic propagation. The results show that the blue-shift observed for lower-order harmonics can be described by a self-phase modulation of the fundamental pulse and not to an intrinsic intensity-dependent phase as discussed by Sekikawa *et al* (2002). This approach should yield a direct measure of the phases of the individual harmonics and permit direct synthesis of a sub-femtosecond train.

The scaled approach is intriguing for another reason: the low binding energy of alkali atoms allows realization of unusual interaction geometries not easily implemented with inert gas atoms. For instance, most excited states of the alkali metal atoms are accessible to visible light. Clatterbuck *et al* (2003) have demonstrated that the high harmonic emission from an excited state is greatly enhanced compared with the ground state. In the experiment, excited states of rubidium atoms are prepared by a weak cw-diode light and are subjected to an intense 3.5 μm mid-infrared pulse. The high harmonic spectrum is explored as a function of state preparation and diode detuning. The enhancement factors are observed to depend on the harmonic order, and increases above the ground state yield are as large as 10^4. These experiments should provide some deeper insights since the HHG process can be controlled at the single atom level.

The use of a long mid-infrared wavelength fundamental field has implications beyond the scaled interactions discussed above. A possible future direction could advance the goal of generating light pulses with not only the atomic timescale (attoseconds) but also the atomic length scale (hard x-rays). Recalling that the ponderomotive energy increases as the square of

the wavelength, a longer wavelength than that of current Ti–sapphire systems will naturally increase the cutoff energy. For example, helium excited by 4 μm pulses will increase the cutoff energy by a factor of 25 over Ti–sapphire, yielding a new cutoff at $\sim$5 keV (2.5 Å). There are obvious drawbacks to this approach, such as an increase in the wave packet spread and a larger variation in the intensity-dependent phase. However, since the single atom will emit in the hard x-ray regime, the low yield may be overcome by the macroscopic propagation. The mid-infrared intensities needed for this strategy do not exist, but advances in parametric amplifiers could result in viable solutions.

5.2. Complete characterization of attosecond pulses

This is clearly a challenge. At the time of writing this, one identifies several proposals for reaching this goal (Muller (2002) through the RABITT method; Itatani *et al* (2002) discuss the principle of an attosecond streak camera able to determine the duration and chirp of a 70 as, pulse while Quéré *et al* (2003) envision using spectral shearing interferometry). Although all these proposals are interesting, and are likely to pave the way to real systems, it is difficult to evaluate their chances at this time. A XUV SPIDER is in progress in several groups, and it is safe to predict that the advent of phase-controlled, few-cycle pump pulses will help enormously in the development of a practical device.

5.3. Attosecond electron pulses and beyond attoseconds

The generation of intense and reproducible attosecond light pulses in the XUV is an exciting goal in itself. However, for many applications the light pulse will be used to excite and control electronic wave packets. Now, the harmonic generation, which is the main source for attosecond light pulses, results itself from an electronic motion launched every half-cycle of the fundamental light (see the three-step model in section 2.3.1). The electron's motion is transformed into photons through a low efficiency process (typically 10^{-8}–10^{-5}). However, the possibility exists of using the electron wave packet itself instead of photons to probe in the sub-femtosecond range and has been demonstrated in a series of experiments (Nikura *et al* 2002, 2003). This topic is beyond the scope of this paper and will not be described further here. It could be remarked, though, that the light pulse, in spite of its many drawbacks, has a number of obvious advantages over the electron wave packet, which, for instance, lacks the capacity to be used at large distances from its origin.

Generation of pulses on the attosecond timescale *per se* is not a physical limit. It is of great interest since electronic motion is scaled in attoseconds (the atomic unit of time is 24 as), but there is no reason why even shorter pulses could not be envisioned. This has been done by Kaplan and Shkolnikov (2002), who proposed the creation of electromagnetic bursts in the 'zepto' (10^{-21}) second timescale by ultra-relativistic electrons in the field of a circularly polarized multipetawatt laser. The future will tell whether this can be actually achieved.

6. Conclusion

Since light pulses are limited by their carrier frequency, visible pulses are bound to a few femtoseconds. XUV or x-ray pulses, on the other hand, allows the transition across the femtosecond border, entering the attosecond timescale. Attosecond pulses, which only a few years ago seemed like wishful thinking, are now effectively generated in the laboratory and have given rise to a number of interesting attophysics applications. It is already clear that

electronic motion can be triggered and controlled by such pulses and many new developments are likely to occur in the near future, as shown by the constant need to update this review as it was being written.

Acknowledgments

LFD acknowledges support under contract No DE-AC02-98CH10886 with the US Department of Energy and support by its Division of Chemical Sciences, Office of Basic Energy Sciences. PA acknowledges the kind hospitality of the Chemistry Department at Brookhaven National Laboratory, where this work was started, and that of FOM-AMOLF, Amsterdam, where it was completed under a Joop Los Fellowship.

References

Antoine Ph *et al* 1996 *Phys. Rev. Lett.* **77** 1234
Antoine Ph *et al* 1997 *Phys. Rev.* A **56** 4960
Apolonski A *et al* 2000 *Phys. Rev. Lett.* **85** 740
Aseyev S A *et al* 2003 *Phys. Rev. Lett.* **91** 223902
Baltuška A *et al* 2002 *Phys. Rev. Lett.* **88** 133901
Baltuška A *et al* 2003 *Nature* **421** 611
Bandrauk A D *et al* 2002 *Phys. Rev. Lett.* **89** 283903
Bandrauk A D *et al* 2002 *Phys. Rev.* A **66** 031401
Bartels R *et al* 2001 *Chem. Phys.* **267** 277
Bloembergen N 1999 *Rev. Mod. Phys.* **71** S283
Bohan A D *et al* 1998 *Phys. Rev. Lett.* **81** 1837
Bouhal A *et al* 1997 *J. Opt. Soc. Am.* B **14** 950
Bouhal A *et al* 1998 *Phys. Rev.* A **58** 389
Brabec T and Krausz F 2000 *Rev. Mod. Phys.* **72** 545
Chang Z *et al* 1997 *Phys. Rev. Lett.* **79** 2967
Chirila C C *et al* 2002 *Phys. Rev.* A **66** 063411
Christov I P *et al* 1997 *Phys. Rev. Lett.* **78** 1251
Christov I P *et al* 1998 *Opt. Commun.* **148** 75
Christov I P *et al* 2001a *J. Opt. Soc. Am.* B **18** 1877
Christov I P *et al* 2001b *Phys. Rev. Lett.* **86** 5458
Cionga A *et al* 1993 *Phys. Rev.* A **47** 1830
Clatterbuck T O *et al* 2003 *J. Mod. Opt.* **50** 441
Clatterbuck T O *et al* 2004 *Phys. Rev.* A submitted
Constant E *et al* 1997 *Phys. Rev.* A **56** 3870
Constant E *et al* 2001 *J. Phys. IV (France)* **11** 537
Corkum P B 1993 *Phys. Rev. Lett.* **71** 1994
Corkum P B *et al* 1994 *Opt. Lett.* **19** 1870
Corkum P B 2000 *Nature* **403** 845
Cormier E and Lambropoulos P 1998 *Eur. Phys. J.* D **2** 15
de Bohan A *et al* 1998 *Phys. Rev. Lett.* **81** 1837
DeMaria A J *et al* 1966 *Appl. Phys. Lett.* **12** 483
Dinu L C *et al* 2003 *Phys. Rev. Lett.* **91** 063901
Drescher M *et al* 2001 *Science* **291** 1923
Drescher M *et al* 2002 *Nature* **419** 803
Duchateau G *et al* 2002 *Phys. Rev.* A **66** 023412
Farkas G and Toth C 1992 *Phys. Lett.* A **168** 447
Ferray M *et al* 1988 *J. Phys. B: At. Mol. Phys.* **21** L31
Fork R L *et al* 1987 *Opt. Lett.* **12** 483
Froehly C *et al* 1973 *J. Opt. (Paris)* **4** 183
Gaarde M B and Schafer K J 2002 *Phys. Rev. Lett.* **89** 213901
Glover T E *et al* 1996 *Phys. Rev. Lett.* **76** 2468

Gouliemakis E *et al* 2002 *Appl. Phys.* B **74** 197
Hänsch T W 1990 *Opt. Commun.* **80** 70
Harris S E *et al* 1990 *Phys. Rev. Lett.* **64** 1107
Harris S E 1994 *Opt. Lett.* **19** 2018
Harris S E *et al* 1993 *Opt. Commun.* **100** 487
Harris S E and Sokolov A V 1997 *Phys. Rev.* A **55** R4019
Harris S E and Sokolov A V 1998 *Phys. Rev. Lett.* **81** 2894
Hellwarth R W 1961 *Bull. Am. Phys. Soc.* **6** 414
Hentschel M *et al* 2001 *Nature* **414** 509
Hertz E *et al* 2001 *Phys. Rev.* A **64** 051801
Hughes S 2000 *Phys. Rev.* A **62** 055401
Iaconis C and Walmsley I 1999 *IEEE J. Quantum Electron.* **35** 501
Itatani J *et al* 2002 *Phys. Rev. Lett.* **88** 173903
Ivanov M *et al* 1995 *Phys. Rev. Lett.* **74** 2933
Jones D J *et al* 2000 *Science* **288** 635
Kalosha V P and Herrmann J 2000 *Phys. Rev. Lett.* **85** 1226
Kaplan A E 1994 *Phys. Rev. Lett.* **73** 1243
Kaplan V P and Shkolnikov L 2002 *Phys. Rev. Lett.* **88** 074801
Kazamias S *et al* 2004 *Phys. Rev.* A at press
Keldysh L V 1965 *Sov. Phys.—JETP* **20** 1307
Kien F L *et al* 2001 *Phys. Rev.* A **64** 051803
Kienberger R *et al* 2002 *Science* **297** 1144
Kienberger R *et al* 2004 *Nature* **427** 817
Kitzler M *et al* 2002 *Phys. Rev. Lett.* **88** 173904
Kovacev M *et al* 2003 *Eur. Phys. J.* D **26** 79
Krause J *et al* 1992 *Phys. Rev. Lett.* **68** 3535
Kuciev Yu 1987 *JETP* **45** 404
Kulander K C *et al* 1993 *Super Intense Laser-Atom Physics* vol 316, ed B Piraux *et al (NATO ASI Ser* B*)* (New York: Plenum) p 95
Lee D G *et al* 2001 *Phys. Rev.* A **63** 021801
Lee K *et al* 2003 *Phys. Rev.* E **67** 026502
Lewenstein M *et al* 1994 *Phys. Rev.* A **49** 2117
L'Huillier *et al* 1991 *J. Phys. B: At. Mol. Opt. Phys.* **24** 3315
Madsen L B *et al* 2002 *Phys. Rev. Lett.* **89** 093202
Mairesse Y *et al* 2003 *Science* **302** 1540
Mashiko H *et al* 2003 *Appl. Phys.* B **76** 525
Muller H G 2001 *Opt. Express* **8** 417
Muller H G 2002 *Appl. Phys.* B **74** S17
McCall S L and Hahn E L 1967 *Phys. Rev. Lett.* **18** 908
McPherson A *et al* 1987 *J. Opt. Soc. Am.* B **4** 595
Milosevic D B and Becker W 2000 *Phys. Rev.* A **62** 011403
Milosevic N *et al* 2002 *Phys. Rev. Lett.* **88** 093905
Nazarkin A *et al* 2002 *Opt. Commun.* **203** 403
Nazarkin A *et al* 2002 *Phys. Rev.* A **65** 041802
Nikura H *et al* 2002 *Nature* **417** 917
Nikura H *et al* 2003 *Nature* **421** 826
Nisoli M *et al* 2003 *Phys. Rev. Lett.* **91** 213905
Norin J T *et al* 2002 *Phys. Rev. Lett.* **88** 193901
Numico R *et al* 2000 *J. Phys. B: At. Mol. Opt. Phys.* **33** 2605
Ohmori K *et al* 2001 *J. Photochem. Photobiol. A: Chem.* **145** 17
Papadogiannis N A *et al* 1999 *Phys. Rev. Lett.* **83** 4289
Papadogiannis N A *et al* 2001 *Phys. Rev. Lett.* **87** 109402
Papadogiannis N A *et al* 2002 *Phys. Rev.* A **66** 025803
Papadogiannis N A *et al* 2003 *Phys. Rev. Lett.* **90** 133902
Paul P M *et al* 2001 *Science* **292** 1689
Peatross J *et al* 1994 *Opt. Lett.* **19** 942
Platonenko V T and Strelkov V V 1999 *J. Opt. Soc. Am.* B **16** 435
Quéré F *et al* 2003 *Phys. Rev. Lett.* **90** 073902

Salières P *et al* 1995 *Phys. Rev. Lett.* **74** 3776
Salières P *et al* 1999 *Adv. At. Mol. Opt. Phys.* **41** 83
Salières P *et al* 2001 *Science* **292** 902
Schafer K J *et al* 1993 *Phys. Rev. Lett.* **70** 1599
Schins J M *et al* 1994 *Phys. Rev. Lett.* **73** 2180
Schins J M *et al* 1996 *J. Opt. Soc. Am.* B **13** 197
Schnürer M *et al* 1998 *Phys. Rev. Lett.* **80** 3236
Sekikawa T *et al* 1999 *Phys. Rev. Lett.* **83** 2564
Sekikawa T *et al* 2002 *Phys. Rev. Lett.* **88** 193902
Shank C V and Ippen E P 1974 *Appl. Phys. Lett.* **24** 273
Sheehy B *et al* 1999 *Phys. Rev. Lett.* **83** 5270
Shon N H *et al* 2002 *Phys. Rev.* A **65** 033809
Shon N H *et al* 2001 *Phys. Rev.* A **63** 063806
Sokolov A V and Harris S E 1997 *Phys. Rev.* A **55** R4019
Sokolov A V *et al* 1999 *Opt. Lett.* **24** 557
Sokolov A V *et al* 2000 *Phys. Rev. Lett.* **85** 562
Sokolov A V *et al* 2001a *Phys. Rev.* A **63** 051801
Sokolov A V *et al* 2001b *Phys. Rev. Lett.* **87** 033402
Staelfeld H *et al* 1996 *Prog. Cryst. Growth Charact. Mater.* **33** 209
Steinmeyer G *et al* 1999 *Science* **286** 1507
Stockman M I 2000 *Phys. Rev.* B **62** 10494
Stupakov G V and Zolotorev M S 2001 *Phys. Rev. Lett.* **86** 5274
Tcherbakov O *et al* 2003 *Phys. Rev.* A **68** 043804
Tempea G *et al* 2001 *Phys. Rev. Lett.* **87** 109401
Toma E S *et al* 2000 *Phys. Rev.* A **62** 0611801
Toma E S and Muller H G 2002 *J. Phys. B: At. Mol. Opt. Phys.* **35** 3435
Trebino R *et al* 1997 *Rev. Sci. Instrum.* **68** 3277
Tzallas P *et al* 2003 *Nature* **426** 267
Vartaka S D and Lawandy N M 1995 *Opt. Commun.* **120** 184
Véniard V *et al* 1996 *Phys. Rev.* A **54** 721
Wittmann M *et al* 2000 *Phys. Rev. Lett.* **84** 5508
Xu L *et al* 1996 *Opt. Lett.* **21** 2008
Yavuz D D *et al* 2000 *Phys. Rev. Lett.* **84** 75
Zewail A H 2000 *J. Phys. Chem.* A **104** 5660
Zhavoronkov N and Korn G 2002 *Phys. Rev. Lett.* **88** 203901